MULTIWAVELENGTH OBSERVATIONS OF TWO MODERATE ROTATION RS CVN SYSTEMS: V815 HERCULES AND IM PEGASI

ROBERT C. DEMPSEY[1,2]

Computer Sciences Corporation,

Space Telescope Science Institute, 3700 San Martin Drive, Baltimore, MD 21218

Electronic mail: dempsey@stsci.edu

JAMES E. NEFF[2,3] and DOUGLAS O'NEAL

The Pennsylvania State University, Department of Astronomy and Astrophysics,

525 Davey Lab, University Park, PA 16802

KATALIN OLAH

Konkoly Observatory, P.O. Box 67, 1525 Budapest, Hungary

FINAL
IN-89-

To Be Submitted to the Astronomical Journal

Draft Date: *March 29, 1995*

Received: _____; *Accepted:* _____

Abstract

[1]Visiting Astronomer, Kitt Peak National Observatory, National Optical Astronomy Observatories, which is operated by AURA, Inc. under cooperative agreement with the National Science Foundation.

[2]Guest Investigator with the International Ultraviolet Explorer satellite, which is sponsored and operated by the National Aeronautics and Space Administration, by the the Science Research Council of the United Kingdom, and by the European Space Agency.

[3]Visiting Astronomer, National Solar Observatory, National Optical Astronomy Observatories, which is operated by AURA, Inc. under cooperative agreement with the National Science Foundation.

Near-to-simultaneous ultraviolet and visual spectroscopy of two moderate $v\sin i$ RS CVn systems, V815 Herculis ($v\sin i = 27$ km s^{-1}) and IM Pegasi ($v\sin i = 24$ km s^{-1}), are presented along with contemporaneous $UBV(RI)_c$-band photometry. These data were used to probe inhomogeneities in the chromospheres and photospheres, and the possible relationship between them. Both systems show evidence for rotationally modulated chromospheric emission, generally varying in anti-phase to the photospheric brightness. A weak flare was observed at Mg II for V815 Her. In the case of IM Peg we use photometry and spectra to estimate temperatures, sizes, and locations of photospheric spots. Further constraints on the spot temperature is provided by TiO observations. For IM Peg, the anticorrelation between chromospheric emission and brightness is discussed in the context of a possible solar-like spot cycle.

Subject headings: stars: chromospheres – binaries: general – stars: late-type – stars: individual: IM Pegasi – stars: individual: V815 Herculis – stars:rotation – stars:activity – stars:variables

1 INTRODUCTION

A very extensive literature details variability of late-type stars in different transitions such as Ca II H and K, Hα, C IV, Mg II, and in radio and X-ray wavelength regions. Variation in the emission in these lines is usually taken as an indication of inhomogeneities in the chromosphere, transition region or corona. Such emission fluctuations are usually accompanied by visual *UBV*-band modulation that is now firmly believed to be the result of large, cool regions located in the photosphere similar to sunspots. In some studies the chromospheric emission varies in antiphase with the photometric wave (increased emission at photometric minimum), which suggests that the active regions are compact and cospatial with spots (e.g., Rodonó et al. 1987; Huenemoerder, Ramsey, & Buzasi 1990; Dempsey et al. 1993a). Just as frequently, however, no correlation or a very complex correlation is observed (e.g., Doyle et al. 1989). Ideally, simultaneous observations should be performed at all wavelengths in order to develop a coherent 3-D atmosphere model. In practice, observations of several proxy indicators simultaneously are rare and tend to focus on the same small number of extremely active systems. Dominating such studies are the RS Canum Venaticorum (RS CVn) and BY Draconis (BY Dra) binaries. The RS CVn systems, first identified by Hall (1976), typically consist of a G- or K-type giant or subgiant with a late-type main sequence or subgiant companion. BY Draconis (BY Dra) binaries contain two late-type main-sequence stars. We have been conducting a campaign to probe surface inhomogeneities on a large number of systems, many with moderate to low levels of activity (Dempsey et al. 1992, 1993a).

In this paper we present near-to-simultaneous visual and ultraviolet observations of two active binaries with very different periods. The first system, V815 Hercules (HD 166181), consists of a solar-like G5 V star tidally locked in a short period (P_{rot} = 1.^{d}8) orbit with an M1-2V companion. Spots are clearly indicated in visual photometric light curves, which typically show a modulation of 0.^{m}13. Dempsey et al. (1993b) found the system to be

X-ray luminous. An X-ray flare has been observed on the system as well as a possible modulation of the X-ray emission due to stellar rotation (Dempsey et al. 1993c; Dempsey et al. 1995). Although it is likely that the spot wave of the visual light curve results from an inhomogeneous photosphere on the G5 V star, it is quite possible that the observed X-ray flare originated on either component.

The second, better studied system, IM Pegasi (HD 216489), contains a K2 III-II primary plus an unknown companion and has an orbital period of 24 days. Dempsey et al. (1994) studied spectral line profile variations in this system and concluded that high-latitude, but not polar, spots were present. IM Peg also exhibits rotational modulation of the Ca II infrared "triplet" (IRT) and Hα emission (Huenemoerder et al. 1990; Dempsey et al. 1993a). Although bright in X-rays, $L_X \sim 42 \times 10^{42}$ erg s^{-1}, no coronal inhomogeneities were detected during the ROSAT All-Sky Survey (Dempsey et al. 1993b, 1995). IM Peg has now been observed in the visual by us over many years. Dempsey et al. (1994) presented preliminary results that IM Peg appear to show a solar-like spot cycle with a period of 12-15 years. Results from the multi-year spot modelling will be presented in full in a later publication.

Ultraviolet observations were obtained with the International Ultraviolet Explorer (IUE) in September through November 1992. Of primary interest were the Mg II h- and k-lines and C IV transition, among others. Walter et al. (1987) and Neff et al. (1989) were able to fit gaussian profiles to the Mg II lines in IUE spectra of AR Lacertae in order to derive a 2-D image of non-uniform chromospheric emission distribution. Visual spectra of V815 Her and IM Peg covered several regions, including Hα and the IRT. Dempsey et al. (1992) used profile assymmetries to model photospheric temperature inhomogeneities, while the chromosphere was probed with the IRT (Dempsey et al. 1993a). Ground based photometry of both stars was obtained at the Konkoly observatory.. In this paper we combine the datasets from the fall of 1992 to obtain a multi-layer snapshot of the outer atmospheres of these two RS CVn systems.

2 OBSERVATIONS

2.1 Visual Spectroscopic Data

Spectroscopic observations for V815 Her and IM Peg were obtained in September 1992 from Kitt Peak National Observatory (KPNO) using the coudé feed telescope. The 1024x1024 TI#3 CCD (**XX**μ pixels) was used with grating A, camera 5 and the long collimator resulting in a two-pixel resolution of 0.32 Å at 6400 Å. Spectra covered Hα, the 8498 and 8542 lines of the IRT, and the 6390–6430 Å region. Additional data for IM Peg were obtained with the National Solar Observatory (NSO). The NSO observations used the Milton-Roy grating #1 (1200 lines/mm) in 2nd order with an 800x800 TI CCD (15 μm pixels) and have a two-pixel resolution of 0.19 Å at Hα. Several spectra of the Hα region with a resolution of 0.11 Å were obtained with the Ritter Observatory 1-m telescope employing a fiber-fed echelle (see Dempsey et al. 1992 for details). Low-resolution ($\Delta\lambda$ 1.24–2.26 Å) echelle observations covering essentially all of the the 4400-9000 Å region were obtained at the Black Moshannon Observatory (BMO). Spectra obtained at NSO and BMO covered the Na I-D and He I lines, Hα, Hβ and several titanium oxide (TiO) bands. The KPNO data were reduced in a standard fashion using IRAF[1]. The NSO data reduction followed the procedures outlined in Neff, O'Neal, & Saar (1995), using IDL routines developed in house but made publicly available. The BMO data reduction used the IDL-based echelle reduction package described by Hall et al. (1994). A log of the visual spectroscopic observations is given in Table 1.

Due to the $v\sin i$ and lower activity levels of the stars studied here, measuring small changes in the line core emission is difficult. For example, equivalent widths usually have

[1]IRAF is distributed by National Optical Astronomy Observatories, which is operated by the Association of Universities for Research in Astronomy, Inc., under contract with the National Science Foundation.

large errors due to uncertainties in continuum placement, definition of the line wings, line blends including those of the secondary, and artifacts such as water vapor lines (Bopp, Dempsey & Maniak 1988). Subtraction of an "inactive" star requires high S/N spectra of stars with identical properties. Here we measure the residual line core intensity, R_c. Bopp et al. (1988), Dempsey (1991), Dempsey et al. (1993a), and Montes et al. (1995) showed how R_c can accurately measure small changes in chromospheric emission of Hα and the IRT. For both systems discussed here, the IRT lines usually have an emission reversal in the high-resolution spectra. In theses cases, R_c is the intensity of the peak core emission divided by the continuum intensity. For the lower-resolution BMO data the emission reversal is generally not visible and in these cases R_C represents the lowest point in the absorption line. Phases for V815 Her were computed from the ephemeris HJD 2,441,930.4877 + 1.8098368E (Strassmeier et al. 1993) and for IM Peg using HJD 2,422,243.316 + 24.39E (Huenmoerder et al. 1990).

2.2 Visual Photometric Data

At Konkoly Observatory $UBV(RI)_C$ photometric observations were made for both systems in August and September of 1992 using the 1m RCC telescope. These data are listed in Tables 2 and 3. Average first and second order extinction coefficients were used. First order standards are from Landolt (1983), and standard magnitudes recalibrated by Menzies (1991).

2.3 Ultraviolet Spectroscopic Data

Ultraviolet spectra were obtained with the International Ultraviolet Explorer (IUE) during the fall of 1992. The IUE observation log is given in Table 4. Both SWP low–resolution and LWP high–resolution spectra were obtained at a number of phases that were intended to evenly cover one rotation cycle of the systems. For V815 Her the spectra were obtained over

15 days, overlapping with the ground-based KPNO observations. IUE spectra for IM Peg were obtained over a 17-day interval and partially overlapped the visual observations. Spectra were extracted and calibrated from the IUE images with the RDAF package of IDL routines. Line fluxes for the emission lines were calculated by least-squares gaussian fits to the line profiles using the ICUR fitting code based on Bevington's (1969) CURFIT (Neff 1987).

3 V815 Her

3.1 Orbit

While measuring wavelengths of some of the visual lines it became apparent that the orbit presented in Nadal et al. (1974) did not accurately predict line positions for our data. We therefore measured 13 radial velocities from the KPNO spectra using the cross-correlation method discussed in Bopp & Dempsey (1989). For the cross-correlations we used the 6390-6430 Å and 6570-6590 Å regions. For standard stars we used μ Her and β Com with radial velocities of -15.9 km s^{-1} and +6.0 km s^{-1}, respectively. Results are listed in Table 5. We estimate the errors of the new velocities to be better than 1 km s^{-1} (Bopp & Dempsey 1989). Overplotting the new data with those from Nadal et al. clearly showed that a systematic shift of approximately 12 km s^{-1} existed between the two sets of radial velocities. To accurately estimate the shift, we calculated the orbit for both the old and new data sets using the standard least-squares program of Bopp, Evans & Lang (1970). From the data of Nadal et al. we find a center of mass velocity, γ, of -13.4 $\pm$ 2.3 km s^{-1} compared to -1.0 $\pm$ 1.5 km s^{-1} for the KPNO observations. Semi-amplitudes, K, of 54.6 $\pm$ 3.3 km s^{-1} and 54.9 $\pm$ 1.2 km s^{-1} were found for the old and new datasets, respectively. Except for γ all new orbital elements were also within errors to the published orbit (see Table 6).

While a systematic error in the velocities of Nadal et al. is possible (e.g., Bopp et al.

1989), such a large offset would be unlikely. A more plausible possibility is that an undetected third body is present in the V815 Her system with an orbit period of many years. Cole et al. (1992) note that a change of 13 km s^{-1} in the center of mass velocity is reasonable for a triple system. The only apparent effect of the third body is to change γ and not any of the other orbital elements.

Since the effect of either possibility is the same from our point of view, we applied a shift to the Nadal et al. data and computed a single "hybrid" orbit. A systematic shift of 12.1 km s^{-1} yielded the smallest residuals, within errors of the $\Delta\gamma$ found above. Errors for the Nadal et al. radial velocities are larger ($\sim$ 3–5 km s^{-1}) than for those derived from cross-correlation and therefore were given an arbitrary weight of 0.8, compared to 1.0 for the KPNO values, when computing the final orbit (see Bopp et al. 1970; Bopp & Dempsey 1989). One value from the Nadal et al. list was consistently poorly fit (O–C $\sim$ 37 km s^{-1}) for any of the computed orbits and was therefore given a weight of 0.0; it's likely that the published sign is in error for this value. The resulting orbit is listed in Table 6 and shown in Figure 1. No significant changes are seen in the orbital elements besides γ, except that it is more clear that the eccentricity is indeed likely zero.

3.2 Visual Data

Due to the low $v\sin i$ (27 km s^{-1}) of the V815 Her primary, the resolution of the visual data is not high enough to detect profile variations. An emission reversal is visible in the IRT lines, shown in Figure 2. The level of activity shown at the IRT is consistent with other active stars with similar periods and spectral types (Dempsey et al. 1993a). Emission filling in the line core of Hα is also evident as seen in Figure 3. Although line core emission is clearly evident in the IRT and Hα profiles (Bopp et al. 1988; Dempsey 1991; Dempsey et al. 1993a; Montes et al. 1995), measurements of R_c did not show any significant variation.

Photometry from September of 1992 is shown in Figure 4. Unfortunately few data points are available, but a minimum appears around phase 0.0 followed by a steep rise to maximum around phase 0.3. The light level is roughly constant until phase 0.8 where it again decreases. Also shown in Fix X are data from August and early September, prior to the UV and optical spectroscopy. These data show that the light curve for V815 Her is highly variable, changing shape dramatically in the space of several weeks ($\approx$ 10 stellar rotations).

3.3 Ultraviolet Data

An example of the LWP high-resolution Mg II spectrum for V815 Her is shown in Figure 5. Phases of conjunction show a single strong Mg II h- and k-line. In several cases, especially at the quadrature phases, emission from both stellar components was resolved. A weak, unresolved interstellar line might be visible in several spectra, but this feature could not be reliably fit. The results of fitting gaussian emission lines and a quadratic background are listed in Table 7. Velocities for the stronger component correspond to the G-star. Based on the fits we conclude that approximately 19% of the Mg II line flux comes from the M-star.

An interesting feature was observed in the red wing of the Mg II lines at phase 1.37 (LWP23980) as seen in Figure 6. This emission was not evident in any other LWP spectrum. Therefore, we conclude that we spectrally resolved a flare on the system. Its position implies redshifts of 60 and 106 km s^{-1} from the G- and M-stars, respectively, either of which may be possible. The Mg II h flux in the flare component was 2.7×10^{-13} erg s^{-1} cm^{-2}. There was no other evidence that the LWP profiles are non-gaussian, as would be the case if the emitting regions were inhomogeneously distributed in the chromosphere. Due to the resolution of IUE and the signal-to-noise of the data we cannot make any conclusions on the spatial distribution of the emitting regions on either star of the V815 Her system based in line profiles.

A representative SWP spectrum of V815 Her is shown in Figure 7. For all features only

a single component can be detected, which is presumed primarily from the G-star. Table 8 lists the SWP line fluxes. Plots of the total fluxes as a function of phase are shown in Figure 8. Significant variations of 20-90% are evident for the SWP fluxes but very little change is seen in the Mg II h-line.

4 IM Peg

4.1 Visual Data

A typical IRT spectrum of IM Peg is shown in Figure 2. The activity level observed in the fall of 1992 is the same as that observed previously (Dempsey et al. 1993a). Variations in the Hα and IRT lines are evident but subtle, as seen in Figure 9. The Hα data, and to a lesser degree the λ8498 data, show clear modulation in anti-phase to the V-band curve (Figure 10). The λ8542 data mimic that for λ8498 but with a smaller amplitude. Too few of the Hβ observations are available to draw any conclusions about variability. Thus IM Peg appears to have retained the clear anti-phase correlation between brightness and chromospheric emission as observed previously by Huenemoerder et al. (1990) and Dempsey et al. (1993a).

Dempsey et al. (1992) first used the Correlative Analysis (CA) technique to estimate the photospheric spot distribution using profile asymmetries combined with photometric modulation. Full details can be found in that paper. In CA, a mean profile is obtained from several lines through cross-correlation with an unspotted template star. The bisector of this mean profile is then modeled using standard methods. Photometry is used in the modelling so that a consistent physical spot model can be derived. In both cases the fitting is done by trial-and-error. In practice any number of spots with any shape and temperature may be used but in practice 2–3 spots at a single temperature is usually adequate. Although simple, Hatzes (1993) derived very similar results with conventional Doppler imaging using very high

S/N data. In a subsequent paper we will present results of multi-season spot modelling of IM Peg, but here we only study the 1992 data.

Originally, Dempsey et al. 1994 used cool spot temperatures, T_{spot}, of 3520 K based on two-spot models by Poe & Eaton 1985 using *VRI* photometry. Based on the TiO data we adopted a T_{spot} of 4000 K for the current modeling. It is not clear whether this really represents an increase in the spot temperature, but a similar effect was observed for σ Geminorum (Dempsey et al. 1992). Using a warmer spot temperature requires larger areas to match the same light curve. Therefore the spot areas presented in Dempsey et al. (1994) would subsequently increase by approximately 40% using T_{spot} of 4000 K. This will be discussed in more detailed in a subsequent publication. For modeling the effective temperature of the primary was taken to be 4500 K and V_o, the maximum brightness, was set at $5^m.60$, the brightest value observed in 17 years of photometric observation. Total spot area is directly related to V_o and it is likely that the value of $5^m.60$ above does not represent a truly unspotted star but rather only the minimum coverage observed to date. TiO observations by Saar, Neff, & O'Neal (1995) further support this conclusion. Little information is added to the modeling processing by using the *UB* photometry (see, for example, Poe & Eaton 1985) so these were not directly used in the modeling. However, the resulting spot model does adequately reproduce the light curves in these bands. Limba darkening coefficients were taken to be 0.73, 0.53 and 0.42 for the *V*-, *R*-, *I*-bands, respectively.

Fits to the 1992 line bisectors are shown in Figure 11. The CA map derived from the 1992 data is displayed in Figure 12. Projected spot areas of 13.8%, 5.2% and 6.7% are derived for the 3 spots shown in the figure. The resulting photometric model is shown in Figure 10 as a solid line.

Neff, O'Neal, and Saar (1995) describe a technique in which the 7100 Å and 8860 Å absorption bands of the TiO molecule are used to determine the area and temperature of

starspots on active stars. Spectra of M giant stars are used to model the spot contribution to the overall active stellar spectrum; both bands become deeper with decreasing effective temperature. For spot temperatures between approximately 3000 K and 3800 K, this technique can independently determine starspot temperature (from the ratio of the strengths of the two bands) and filling factor (from their absolute depths). The upper temperature limit for this technique is set by the temperature at which the 8860 Å TiO band is first observable.

On IM Peg, this spectroscopic technique is complicated by three factors. First only 4 observations between phase 0.99–0.14 were obtained. Second, no absorption was measured in the 8860 Å TiO band, thus the starspots appear to be warmer than 3800 K. This eliminates one of the constraints needed to independently derive starspot filling factor and temperature. Finally, IM Peg is a K2 giant, a star cool enough to show measurable absorption in the 7100 Å TiO bands even from the unspotted photosphere. Inactive K2 III comparison stars show a depth of 1.0 to 1.5% in the leading 7100 Å TiO band.

The first TiO band observation was taken at phase 0.99; this is approaching the deeper of the two photometric minima. At phases 0.02 and 0.11 the TiO strengths indicate spot filling factors of 2.3% and 1.9%, respectively. By phase 0.14 the derived spot coverage increased to 12%. See Figure 13. In deriving these starspot filling factors, we assumed that the lowest observed 7100Å depth of 1.3% at phase 0.99 represents no spot coverage and that the temperature of the spots is 4000 K. Even if these assumptions are incorrect, the technique yields approximately correct relative spot coverages.

The TiO observations are easily understandable in terms of the map in Figure 12. Near phase 0.99, only a small portion of the largest spot is in view and with foreshortening and limb darkening, the TiO area should be a minimum. Towards phase 0.15 the spot is fully in view consistent with the larger derived spot filling factor. Unfortunately, no TiO observations were obtained at the later phases.

4.2 Ultraviolet Data

Huenemoerder et al. (1990) first studied the UV variability of IM Peg using 10 IUE spectra obtained during the summers of 1985 and 1986. They found the UV fluxes to vary in phase with the Ca II IRT emission. Our IUE observations (see Table 4) were planned to cover one complete rotation in as short a time as possible. Figures 14 and 15 show typical LWP and SWP spectra of IM Peg, respectively. For the Mg II profiles we attempted single and multiple gaussian fits to the emission along with a single gaussian for the interstellar absorption. None of the LWP spectra show any evidence of emission from the secondary and in all cases the single emission gaussian fit the data well. All SWP emission lines were also well fit with single gaussians.

Line fluxes as a function of phase are given in Tables 9 and 10 and shown in Figure 16. The Mg II h- and k-lines showed no significant fluctuation over the rotational cycle. Small changes are seen in the SWP line fluxes. The Si III] and C III] line ratio can be used to estimate the electron density, N_e, of the emitting plasma. Signal-to-noise is poor for these lines in our spectra so error bars are large. From Keenan, Dufton & Kingston (1987) we estimate that $N_e \approx 10^{10}$ cm^{-3}, with a density at phase 0.8 a factor of 3 lower. Although the line fluxes vary in IM Peg, there is no evidence for asymmetries in the UV line profiles themselves.

5 DISCUSSION

The V815 Her UV line fluxes and the IRT emission are indicative of a very active star (Hartmann, Dupree, & Raymond 1982; Dempsey et al. 1993a). Generally, the UV line fluxes show a decrease during the early rotational phases followed by an increase after phase 0.6. This trend is exactly the opposite of that seen in the photometry shown in Fig. 4. Such behavior is reminiscent of the more traditional solar paradigm with chromospheric emission

varying with an anticorrelation to photospheric brightness, i.e. chromospheric optical and UV emission from regions cospatial with spots in the photosphere. Most stellar systems studied in this manner either do not show such a correlation or, in some cases, show a clear correlation one season and then do not at another epoch. Such is the case of the similar RS CVn, σ Geminorium (K1 III, $P_{rot} = 19^d$), studied over two seasons (Dempsey et al. 1993a).

For V815 Her the large UV flux variability, including possible flares, superimposed on a weakly modulated signal is qualitatively similar to the behavior observed in the X-ray light curve obtained by ROSAT two years earlier (Dempsey et al. 1993c). This does not, however, imply a long term correlation, as the August photometry clearly shows that the V815 Her system is highly variable. Lines formed in the lower chromosphere (e.g., Mg II, Si II, Hα, IRT) show the weakest modulation or none altogether. Flaring activity, as indicated by the Mg II data presented here and the X-ray data presented in Dempsey et al. (1993c) and Dempsey et al. (1995), appears to be common on one or both components in the V815 Her system.

The anticorrelation between photometric brightness and UV emission is more evident in IM Peg. The IM Peg anticorrelation was also the observed in IRT data in 1985 and 1986 (Huenemoerder et al. 1990) and 1989 (Dempsey et al. 1993a) suggesting the phenomenon is relatively stable. However, even this is over simplified. While Huenemoerder et al. (1990) observed Hα to be essentially constant in the summers of 1985 and 1986, we do observe a significant modulation in the Hα emission. Dempsey et al. (1994) tentatively identified a solar-like cycle on IM Peg based on 15 years of photometry. If valid, the Huenemoerder et al. Hα observations would roughly correspond to the spot minimum phase of the cycle, while those reported here occurred during spot maximum. This suggests a possible change in the chromospheric network over the cycle.

The authors thank B. W. Bopp for providing the Ritter Observatory spectra and for G. W. Henry for sharing the APT data. Research at CSC has been supported by NASA grant NAS5-32616. RCD wishes to thank S. Osmer and M. Dew for help in preparing the manuscript. Research at Penn State University was partially funded through NASA grant NAGW-2603.

REFERENCES

Bevington, P. R., 1969, Data Reduction and Error Analysis for the Physical Science (McGraw-Hill: New York)

Bopp, B. W. & Dempsey, R. C. 1989, PASP, 101, 516

Bopp, B. W., Dempsey, R. C. & Maniak, S. 1988, ApJS, 68, 803

Bopp, B. W., Evans, D. S. & Lang, J. D. 1970, MNRAS, 147, 355

Bopp, B. W., Saar, S. H., Ambruster, C. W., Feldman, P., Dempsey, R. C., Allen, M. & Barden, S. 1989, ApJ, 339, 1059

Cole, W. A., Fekel, F. C., Hartkopf, W. I., McAlister, H. A. & Tomkin, J. 1992, AJ, 103, 1357

Dempsey, R. C., 1991, Ph D thesis, University of Toledo, Toledo, OH

Dempsey R. C., Bopp, B. W., Strassmeier, K. G., Granados, A. F., Henry, G. W. & Hall, D. S., 1992, ApJ, 392, 187

Dempsey R. C., Bopp, B. W., Henry, G. W. & Hall, D. S. 1993a, ApJS, 86, 293

Dempsey, R. C., Linsky, J. L, Fleming, T. A. & Schmitt, J. H. M. M. 1993b, ApJS, 86, 599

Dempsey, R. C., Linsky, J. L., Fleming, T. A., Schmitt, J. H. M. M. & Kürster, M. 1993c, in Physics of Solar and Stellar Coronae, ed. J. L. Linsky and S. Serio, (Dordrecht: Kluwer), 361

Dempsey, R. C., Bopp, B. W., Henry, G. W. & Hall, D. 1994, in Cool Stars, Stellar Systems, and the Sun, ed. J.-P. Caillault, ASP Conference Series, 64, 393

Dempsey, R. C., Linsky, J. L, Schmitt, J. H. M. M. & Kürster, M. 1995, ApJS, in preparation

Doyle, J. G., Butler, C. J., Byrne, P. B., Rodonó, M., Swank, J. & Fowles, W. 1989, A&A, 223, 219

Genet, R. M., Boyd, L. J., Kissell, K. E., Crawford, D. L., Hall, D. S., Kayes, D. S. & Baliunas, S. L. 1987, PASP, 99, 660

Hall, D. S. 1976, in IAU Colloq. 29, Multiply Periodic Phenomena in Variable Stars, ed. W. S. Fitch (Dordrecht: Reidel), 287

Hall, J. C., Fulton, E. E., Huenemoerder, D. P., Welty, A. D., Neff, J.E. 1994, PASP, 106, 315

Hartmann, L., Dupree, A. K. & Raymond, J. C. 1982, ApJ, 252, 214

Hatzes, A. P. 1993, ApJ, 410, 777

Huenemoerder, D., Ramsey, L., & Buzasi, D. 1990, ApJ, 350, 763

Keenan, F. P., Dufton, P. L. & Kingston, A. E. 1987, MNRAS, 225, 859

Landolt, A.U., 1983, AJ 88,439

Menzies, J.W. et al, 1991, MNRAS 248, 642

Montes, D., Fernández-Figueroa, M. J., De Castro, E. & Cornide, M. 1995, A&A 294, 165

Neff, J. E. 1987, Ph. D. thesis, University of Colorado, Boulder

Neff, J. E., O'Neal, D., Saar, S. H. 1995, ApJ, submitted

Neff, J. E., Walter, F. M., Rodonó, M. & Linsky, J. L. 1989, A&A 215, 79

Nadal, R., Pedoussaut, A., Ginestet, N. & Carquillat, J. M. 1974, A&A 37, 191

Poe, C. H. & Eaton, J., A. 1985, ApJ, 289, 644

Rodonó, M., Byrne, P. B., Neff, J. E., Linsky, J. L., Simon, T., Butler, C. J., Catalano, S., Cutispoto, G., Doyle, J. G., Andrews, A. D. & Gibson, D. M. 1987, A&A, 176, 267

Strassmeier, K. G., Hall, D. S., Fekel, F. C. & Scheck, M. 1993, A&AS, 100, 173

Walter, F. M., Neff, J. E., Gibson, D. M., Linsky, J. L., Rodonó, M., Gary, D. E. & Butler, C. J. 1987, A&A 186, 241

This manuscript was prepared with the AAS WGAS LaTeX macros v2.2

Figure 1: Radial velocities for V815 Her (+'s are from this paper, *'s are from Nadal et al.) with final combined orbital solution (solid line). The value near phase 0.2 with an O-C of 40 km s^{-1} is believed to be a misprint and was not used in the solutions.

Figure 2: IRT region of V815 Her (middle spectrum), IM Peg (top spectrum) and the standard star α Arietis (K2 III, bottom spectrum). Emission reversals are clearly seen in the λ 8498 and λ 8542 lines in both of the RS CVn spectra. Spectra have been normalized to unity and the upper two shifted arbitrarily in the vertical direction for clarity.

Figure 3: HI Balmer-α region of V815 Her (middle spectrum), IM Peg (top) and α Ari (bottom). Note that the shallowness of the line cores in V815 Her and IM Peg result from both rotational broadening and chromospheric emission (see further Bopp, Dempsey & Maniak 1988; Dempsey 1991). Spectra have been normalized to unity and the upper two shifted arbitrarily in the vertical direction for clarity.

Figure 4: *V*-band light curve for V815 Her from August and early September (top) and for later September when the IUE observations were obtained (bottom).

Figure 5: Sample LWP spectrum for V815 Her. The spectrum (LWP24075) represents a typical or "quiescent" level (see also Fig. 5).

Figure 6: Model fit to the Mg II h-line for LWP23980. The most blueward component is from the secondary while the strongest profile arises from the primary. The reward component is attributed to a flare.

Figure 7: Sample SWP spectrum for V815 Her. Several prominent lines are identified. The heavy "X"s along the bottom indicate camera reseau marks.

Figure 8: IUE fluxes versus phase for several transitions in V815 Her. In the bottom panel, the left- and right-hand y-axis labels correspond to the C IV and Mg II fluxes, respectively. For Si II and Si IV the flux is the sum of both lines listed in Table 8.

Figure 9: (a) R_c for λ8498 (asterisks) and Hα (pluses and diamonds) for IM Peg. For Hα, pluses indicate KPNO and NSO data while the diamonds represent the RO data. Values of R_c for λ8542 are similar to those of λ8498 but with a smaller amplitude in the variation. (b) Data from BMO are shown in the bottom panel. Asterisks and triangles represent IRT data from August and September, respectively. R_c for Hα is designated by pluses and diamonds for the August and September data, respectively.

Figure 10: *V*-band (top) and *I*-band light curves for IM Peg from fall of 1992. The solid line represents the spot model displayed in Fig. 12 and discussed below. Similar results are observed for the *UBR*-band light curves.

Figure 11: The observed and theoretical bisectors for IM Peg. Model bisectors are fitted by eye using a trial and error method.

Figure 12: Resulting spot map for IM Peg. Dark shaded regions indicate a uniform T_{spot} of 4000 K.

Figure 13: 7100 Å region spectrum of IM Peg taken at phase=0.14. Arrows indicate positions of the 7055 Å, 7088 Å, and 7126 Å bandheads of TiO. This spectrum exhibits the deepest TiO bands among our IM Peg observations.

Figure 14: Sample LWP spectrum for IM Peg.

Figure 15: Sample SWP spectrum for IM Peg. The heavy "X"s along the bottom indicate camera reseau marks.

Figure 16: IUE fluxes versus phase for IM Peg. For Si II and Si IV the flux is the sum of both lines listed in Table 10.

Table 1: Log of Visual Observations

Target	UT Date	Exposure (Sec)	UT Start	Region	Observatory[a]
IM Peg	02-aug-1992	900	07:17	echelle	BMO
IM Peg	03-aug-1992	900	07:02	echelle	BMO
IM Peg	05-aug-1992	900	06:51	echelle	BMO
IM Peg	06-aug-1992	600	06:52	echelle	BMO
IM Peg	07-aug-1992	900	06:33	echelle	BMO
IM Peg	12-aug-1992	900	05:22	echelle	BMO
IM Peg	20-aug-1992	900	04:27	echelle	BMO
IM Peg	22-aug-1992	900	05:39	echelle	BMO
V815 Her	11-sep-1992	1800	02:49	Hα	NSO
IM Peg		900	04:06	Hα	NSO
IM Peg		600	08:12	Hβ	NSO
IM Peg	12-sep-1992	600	07:16	Hα	NSO
IM Peg		600	10:54	Hβ	NSO
IM Peg	14-sep-1992	420	07:25	Hα	NSO
IM Peg		600	11:07	Hβ	NSO
IM Peg	14-sep-1992	420	07:53	Hα	NSO
IM Peg	16-sep-1992	480	08:14	Hα	NSO
V815 Her	22-sep-1992	2000	02:16	6420	CF
IM Peg		600	04:05	6420	CF
V815 Her		1800	04:38	6420	CF
V815 Her		1800	05:28	IRT	CF
IM Peg		2700	06:56	IRT	CF
IM Peg		300	09:24	Hα	CF
V815 Her	23-sep-1992	1800	02:18	IRT	CF
V815 Her		2100	02:58	6420	CF
IM Peg		300	06:39	Hα	CF
IM Peg		1200	07:41	IRT	CF
V815 Her	24-sep-1992	2100	02:09	IRT	CF
V815 Her		2000	03:50	6420	CF
V815 Her		900	04:50	Hα	CF
IM Peg		300	05:38	Hα	CF
IM Peg		300	06:46	6420	CF
V815 Her	25-sep-1992	2100	02:15	IRT	CF
V815 Her		2000	03:50	6420	CF
V815 Her		900	04:50	Hα	CF
IM Peg		300	05:44	Hα	CF
IM Peg		300	06:50	6420	CF
IM Peg		1200	07:51	IRT	CF

Table 1: Log of Visual Observations (continued)

Target	UT Date	Exposure (Sec)	UT Start	Region	Observatory[a]
V815 Her	26-sep-1992	2100	02:09	IRT	CF
V815 Her		2000	03:29	6420	CF
V815 Her		1000	05:25	Hα	CF
IM Peg		300	06:06	Hα	CF
IM Peg		1200	06:49	IRT	CF
IM Peg		300	08:12	6420	CF
V815 Her	27-sep-1992	2000	02:04	IRT	CF
V815 Her		2000	03:48	6420	CF
V815 Her		1000	05:24	Hα	CF
IM Peg		300	06:04	Hα	CF
V815 Her	28-sep-1992	1800	02:34	IRT	CF
V815 Her		2000	03:58	6420	CF
V815 Her		900	04:55	Hα	CF
IM Peg		300	05:30	Hα	CF
IM Peg		1500	06:43	IRT	CF
IM Peg		400	08:10	6420	CF
IM Peg	14-oct-1992	450	02:34	echelle	BMO
IM Peg	22-oct-1992	3000	02:20	Hα	RO
IM Peg	25-oct-1992	2500	01:24	Hα	RO
IM Peg	26-oct-1992	2500	01:30	Hα	RO
IM Peg	27-oct-1992	450	02:07	echelle	BMO
IM Peg	27-oct-1992	1200	02:45	echelle	BMO
IM Peg	27-oct-1992	450	02:07	echelle	BMO
IM Peg	28-oct-1992	600	02:19	echelle	BMO
IM Peg	28-oct-1992	600	02:31	echelle	BMO
IM Peg	28-oct-1992	600	02:41	echelle	BMO
IM Peg	28-oct-1992	600	02:51	echelle	BMO
IM Peg	29-oct-1992	600	01:42	echelle	BMO
IM Peg	29-oct-1992	600	01:53	echelle	BMO
IM Peg	29-oct-1992	600	02:03	echelle	BMO
IM Peg	29-oct-1992	600	02:14	echelle	BMO
IM Peg	08-nov-1992	420	02:50	echelle	BMO
IM Peg	08-nov-1992	420	02:57	echelle	BMO
IM Peg	08-nov-1992	420	03:05	echelle	BMO

[a]NSO indicates the National Solar Observatory observations, CF are the Coudé Feed spectra, RO designates Ritter Observatory, and BMO designates Black Moshannon Observatory.

Table 2: V815 Her Photometry

HJD	Phase	ΔV^a	*(U-B)*	*(B-V)*	*(V-I)*	*(V-R)*
48748.4219	0.15	0.863	0.103	0.079	0.174	0.079
48798.4414	0.79	0.859	0.094	0.080	0.165	0.068
48800.4141	0.88	0.882	0.089	0.085	0.181	0.078
48801.4102	0.43	0.855	0.092	0.077	0.172	0.074
48802.5469	0.06	0.875	0.089	0.081	0.173	0.076
48803.5391	0.61	0.841	0.104	0.080	0.162	0.074
48804.4609	0.12	0.866	0.097	0.079	0.176	0.077
48805.4062	0.64	0.832	0.093	0.081	0.168	0.071
48808.5391	0.37	0.872	0.087	0.079	0.176	0.077
48859.3555	0.45	0.868	0.086	0.089	0.175	0.079
48860.3789	0.01	0.867	0.090	0.084	0.173	0.067
48861.3789	0.57	0.875	0.087	0.079	0.169	0.073
48883.3633	0.71	0.835	0.090	0.071	0.165	0.070
48884.2617	0.21	0.854	0.088	0.077	0.170	0.074
48885.2734	0.77	0.851	0.091	0.079	0.169	0.073
48886.2734	0.32	0.838	0.080	0.076	0.167	0.070
48888.2539	0.42	0.837	0.084	0.081	0.158	0.066
48888.2812	0.43	0.836	0.086	0.074	0.159	0.071
48890.3516	0.58	0.837	0.076	0.078	0.160	0.071
48891.2461	0.07	0.890	0.096	0.084	0.182	0.074
48892.2500	0.62	0.840	0.080	0.078	0.165	0.070
Mean		0.856	0.900	0.080	0.170	0.073
σ		0.017	0.007	0.004	0.006	0.004

[a]Differential photometry using comparison star BD +29° 3190 V=6.85 U-B=0.22 B-V=0.64 V-R_c=0.34 V-I_c=0.71

Table 3: IM Peg Photometry

HJD	Phase	ΔV[a]	*(U-B)*	*(B-V)*	*(V-I)*	*(V-R)*
48859.4453	0.27	-0.795	0.204	0.131	0.116	0.086
48860.6016	0.32	-0.792	0.192	0.124	0.117	0.084
48862.5625	0.40	-0.759	0.196	0.136	0.132	0.090
48863.5703	0.44	-0.732	0.200	0.140	0.133	0.097
48883.5000	0.26	-0.779	0.207	0.123	0.127	0.091
48886.3906	0.38	-0.765	0.204	0.132	0.135	0.095
48888.4336	0.46	-0.730	0.212	0.143	0.142	0.095
48890.4258	0.54	-0.701	0.202	0.143	0.146	0.098
48891.3789	0.58	-0.701	0.205	0.149	0.154	0.099
48892.5273	0.63	-0.693	0.206	0.138	0.150	0.098
48897.4102	0.83	-0.705	0.206	0.132	0.152	0.095
48954.1953	0.16	-0.701	0.215	0.136	0.158	0.106
48954.3164	0.16	-0.689	0.213	0.126	0.159	0.103
48956.1914	0.24	-0.757	0.211	0.128	0.133	0.090
48957.3242	0.29	-0.780	0.203	0.128	0.127	0.089
48974.2773	0.98	-0.666	0.208	0.133	0.164	0.109
48975.1875	0.02	-0.659	0.199	0.142	0.164	0.101
48979.1680	0.18	-0.715	0.202	0.143	0.153	0.094
Mean		-0.729	0.205	0.135	0.142	0.096
σ		0.042	0.006	0.007	0.015	0.006

[a]Differential photometry using comparison star HD 216635 V=6.617 U-B=0.74 B-V=1.04 V-R_c=0.555 V-I_c=1.053.

Table 4: Log of IUE Observations

Image	Target	UT Exposure Start	Duration (Seconds)
LWP 23976	V815 Her	20-sep-1992 03:46:12	1800.000
SWP 45689	V815 Her	20-sep-1992 04:23:17	9000.000
LWP 23980	V815 Her	22-sep-1992 03:54:57	1800.000
SWP 45740	V815 Her	22-sep-1992 04:33:01	8400.000
LWP 23988	V815 Her	23-sep-1992 03:05:24	1800.000
SWP 45752	V815 Her	23-sep-1992 03:40:18	11100.000
LWP 23993	V815 Her	24-sep-1992 03:36:12	1800.000
SWP 45764	V815 Her	24-sep-1992 04:11:28	9600.000
LWP 24000	V815 Her	25-sep-1992 03:31:55	1800.000
SWP 45768	V815 Her	25-sep-1992 04:07:28	9720.000
LWP 24005	V815 Her	26-sep-1992 03:43:53	1800.000
SWP 45775	V815 Her	26-sep-1992 04:18:55	9000.000
LWP 24010	V815 Her	27-sep-1992 03:45:47	1800.000
SWP 45782	V815 Her	27-sep-1992 04:20:34	9000.000
LWP 24018	V815 Her	28-sep-1992 03:33:04	1800.000
SWP 45785	V815 Her	28-sep-1992 04:08:10	9823.000
LWP 24075	V815 Her	05-oct-1992 01:40:06	1800.000
SWP 45842	V815 Her	05-oct-1992 02:14:55	9300.000
LWP 24134	IM Peg	22-oct-1992 10:18:55	1800.000
SWP 46035	IM Peg	22-oct-1992 10:55:28	5400.000
LWP 24135	IM Peg	22-oct-1992 12:31:53	1080.000
LWP 24141	IM Peg	24-oct-1992 10:09:10	1800.000
SWP 46049	IM Peg	24-oct-1992 10:45:02	5400.000
LWP 24142	IM Peg	24-oct-1992 12:26:56	1200.000
LWP 24156	IM Peg	26-oct-1992 09:35:08	1800.000
SWP 46066	IM Peg	26-oct-1992 10:13:18	5400.000
LWP 24157	IM Peg	26-oct-1992 11:47:56	1200.000
SWP 46067	IM Peg	26-oct-1992 12:19:11	1800.000
LWP 24171	IM Peg	28-oct-1992 10:00:28	1800.000
SWP 46084	IM Peg	28-oct-1992 10:38:38	6600.000
LWP 24172	IM Peg	28-oct-1992 12:33:32	960.000

(continued)

Table 5: Log of IUE Observations (continued)

Image	Target	UT Exposure Start	Duration (Seconds)
LWP 24193	IM Peg	30-oct-1992 09:31:21	1800.000
SWP 46098	IM Peg	30-oct-1992 10:14:19	6600.000
LWP 24194	IM Peg	30-oct-1992 12:13:03	1200.000
SWP 46120	IM Peg	03-nov-1992 07:44:52	6600.000
LWP 24249	IM Peg	03-nov-1992 07:19:52	1200.000
LWP 24250	IM Peg	03-nov-1992 09:45:00	1500.000
LWP 24290	IM Peg	07-nov-1992 07:59:00	1500.000
SWP 46150	IM Peg	07-nov-1992 08:29:47	6600.000

Table 6: V815 Her Radial Velocities

HJD	Phase	RV km s^{-1}	Weight	O-C km s^{-1}
2432760.6650	0.1592	-44.20	0.8	2.28
2433136.5870	0.8699	-19.10	0.8	-0.84
2433507.6530	0.8975	-20.60	0.8	6.73
2433772.8750	0.4423	42.90	0.8	5.82
2434303.5210	0.6437	41.50	0.8	-5.37
2441840.5790	0.1445	-11.80	0.0	37.53
2441488.5390	0.6295	50.70	0.8	1.98
2441812.5380	0.6508	45.20	0.8	-0.62
2441864.4600	0.3396	7.80	0.0	-0.04
2441865.4540	0.8888	-23.00	0.8	1.55
2441866.5030	0.4684	41.60	0.8	-0.85
2441867.4550	0.9944	-49.10	0.8	2.18
2441868.5410	0.5945	53.70	0.8	2.11
2441869.5570	0.1559	-49.80	0.8	-2.64
2441870.4800	0.6659	42.70	0.8	-0.57
2441930.3330	0.7368	20.70	0.8	-5.57
2441930.4880	0.8225	1.20	0.8	2.99
2441931.3220	0.2833	-14.20	0.8	-3.25
2441932.3370	0.8441	-9.40	0.8	-0.03
2441933.3340	0.3950	23.40	0.8	-1.53
2441934.3280	0.9442	-45.40	0.8	-4.60
2441935.4240	0.5498	50.10	0.8	-1.69
2441936.3400	0.0559	-58.60	0.8	-1.84
2448678.9941	0.6194	52.20	1.0	2.42
2448679.9753	0.1616	-42.20	1.0	3.79
2448681.0076	0.7319	31.80	1.0	4.13
2448681.9170	0.2344	-23.40	1.0	3.35
2448887.6062	0.8852	-26.50	1.0	-3.12
2448888.6359	0.4542	36.40	1.0	-3.25
2448889.6713	0.0263	-55.70	1.0	-0.49
2448889.7066	0.0458	-57.20	1.0	-0.74
2448890.6713	0.5788	52.30	1.0	0.19
2448890.7066	0.5983	54.70	1.0	3.31
2448891.6566	0.1232	-53.80	1.0	-1.13
2448892.6698	0.6831	36.40	1.0	-3.47

Table 7: Orbital Solutions

Dataset	γ km s^{-1}	K km s^{-1}	e	ω deg	T_o	P_{orb} days
Nadal et al.	-13.4	54.6	0.03	219.1	2,441,931.13	1.8098369
$\pm$	2.3	3.3	0.05	132.7	0.67	0.0000083
KPNO	-1.6	54.9	0.05	103.2	2,441,926.80	1.8098664
$\pm$	1.0	1.2	0.02	28.9	0.56	0.0001400
Both	-1.0	54.5	0.02	156.0	2,441,929.00	1.8098347
$\pm$	1.5	1.9	0.04	79.1	0.39	0.0000039

Table 8: V815 Her MgII Fluxes[a]

LWP	JD (+2440000)	Phase	h_1[b]	h_2	h_f
			2803 Å		
23976	8886.1681	0.26	0.93	0.22	
23980	8888.1736	1.37	0.65	0.14	0.27
23988	8889.1396	1.90	0.96		
23993	8890.1611	2.47	1.08		
24000	8891.1576	3.02	1.18		
24005	8892.1660	3.58	1.03		
24010	8893.1674	4.13	1.23		
24018	8894.1583	4.68	0.57	0.14	
24075	8901.0799	8.50	0.93		
Mean[c]			1.01		
σ[d]			0.06		

[a]Fluxes are in units of 10^{-12} erg s^{-1} cm^{-2}.

[b]The numbers 1 and 2 designate the G- and M-stars, respectively, while the f subscript indicates the flare component.

[c]Two-components were added for computing the mean and σ.

[d]Standard deviation of the mean.

Table 9: V815 Her SWP Fluxes[a]

SWP	JD (+2440000)	Phase	O I 1305	C II 1335	Si IV 1396	Si IV 1402	C IV 1550	He II 1640	C I[b] 1658	Si II 1808	Si II 1817
45689	8886.2354	0.30	0.49	0.65	0.82	0.30	2.92	1.67	0.65	0.94	0.52
45740	8888.2383	1.41	0.31	1.10	0.63	0.33	2.87	1.72	1.10	1.34	–
45752	8889.2178	1.95	0.58	1.05	0.52	0.55	3.69	1.96	1.05	0.93	0.27
45764	8890.2305	2.51	0.12	1.05	0.55	0.35	3.47	1.77	1.05	0.95	0.58
45768	8891.2285	3.06	0.80	1.41	0.81	0.57	4.38	2.18	1.41	0.79	0.58
45775	8892.2314	3.61	0.56	1.65	0.77	0.74	3.39	1.76	1.65	0.89	0.26
45782	8893.2334	4.17	0.67	1.33	0.73	0.31	3.34	1.67	1.33	1.00	0.29
45785	8894.2295	4.72	0.63	0.92	0.63	0.49	3.97	1.83	0.92	1.01	0.67
45842	8901.1475	8.54	0.62	1.27	0.83	0.58	2.94	1.66	1.27	0.90	0.65
Mean			0.53	1.16	0.70	0.47	3.44	1.80	1.16	0.97	0.48
σ			0.06	0.09	0.04	0.05	0.16	0.05	0.09	0.05	0.06

[a] Fluxes are in units of 10^{-13} erg s^{-1} cm^{-2}.

[b] Blended line.

Table 10: IM Peg Mg II Fluxes[a]

LWP	JD (+2440000)	Phase	F_h 2803 Å	F_k 2795 Å
24134+24135	8917.9766	0.67	1.63	2.21
24141+24142	8919.9688	0.75	1.68	2.23
24156+24157	8921.9453	0.83	1.68	2.18
24171+24172	8923.9688	0.92	1.68	2.18
24193+24194	8925.9531	1.00	1.59	2.15
24249+24250	8929.8555	0.16	1.70	2.09
24290+24291	8933.8828	0.32	1.73	2.34
Mean			1.67	2.20
σ			0.02	0.03

[a]Fluxes are in units of 10^{-11} erg s^{-1} cm^{-2}.

Table 11: IM Peg SWP Fluxes[a]

SWP	JD (+2440000)	Phase	O I 1305	C II 1335	Si IV 1396	Si IV 1402	C IV 1550	He II 1640	C I[b] 1658	Si II 1808	Si II 1817	Si III] 1893	C III] 1909
46035	8917.9551	0.67	15.98	4.02	2.25	2.17	9.65	4.70	4.02	7.07	3.06	2.75	1.68
46049	8919.9482	0.75	16.66	5.93	4.32	4.65	17.33	8.94	5.93	7.31	3.65	3.02	1.84
46066	8921.9258	0.83	17.50	5.07	2.98	2.10	8.94	8.36	5.07	7.31	3.65	5.44	1.83
46067	8922.0137	0.84	–	4.80	3.49	2.93	16.13	6.35	4.80	7.36	3.61	5.13	1.92
46084	8923.9434	0.92	–	5.96	4.64	3.49	16.40	–	5.96	8.53	3.48	3.82	2.93
46098	8925.9268	1.00	–	6.29	5.46	3.90	–	7.93	6.29	–	–	4.14	1.85
46120	8929.8223	0.16	–	5.14	3.79	2.92	16.13	7.05	5.14	7.54	3.23	4.92	2.33
46150	8933.8535	0.32	14.99	4.25	3.16	4.30	14.22	8.13	4.25	7.35	4.78	4.09	3.47
Mean		0.69	16.28	5.18	3.76	3.31	14.11	7.35	5.18	7.50	3.64	4.16	2.23
σ		0.10	0.46	0.27	0.34	0.31	1.20	0.51	0.27	0.17	0.19	0.32	0.21

[a]Fluxes are in units of 10^{-13} erg s^{-1} cm^{-2}.

[b]Blended line

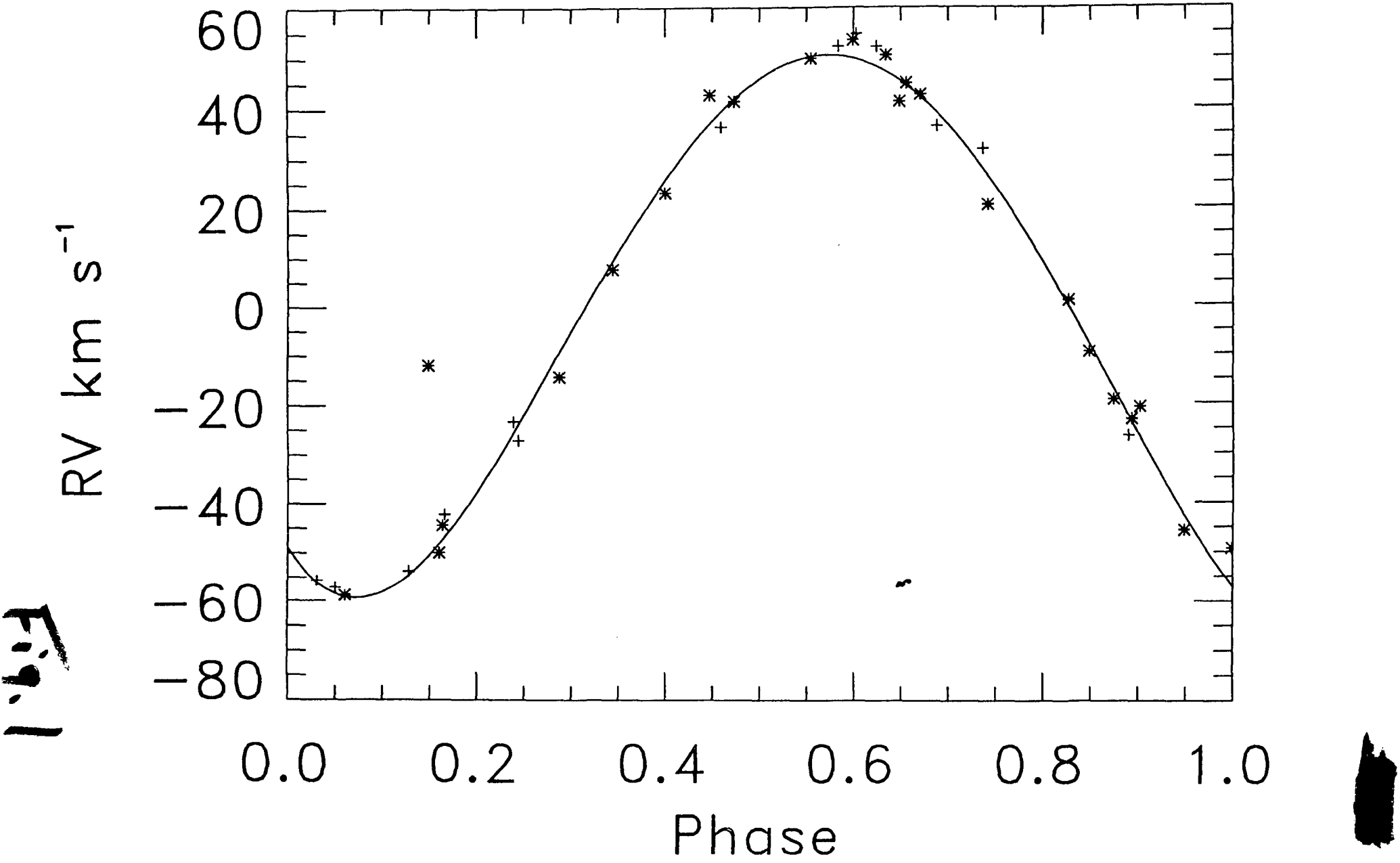
60
40
20
0
−20
−40
−60
−80
RV km s^{-1}
0.0
0.2
0.4
0.6
0.8
1.0
Phase

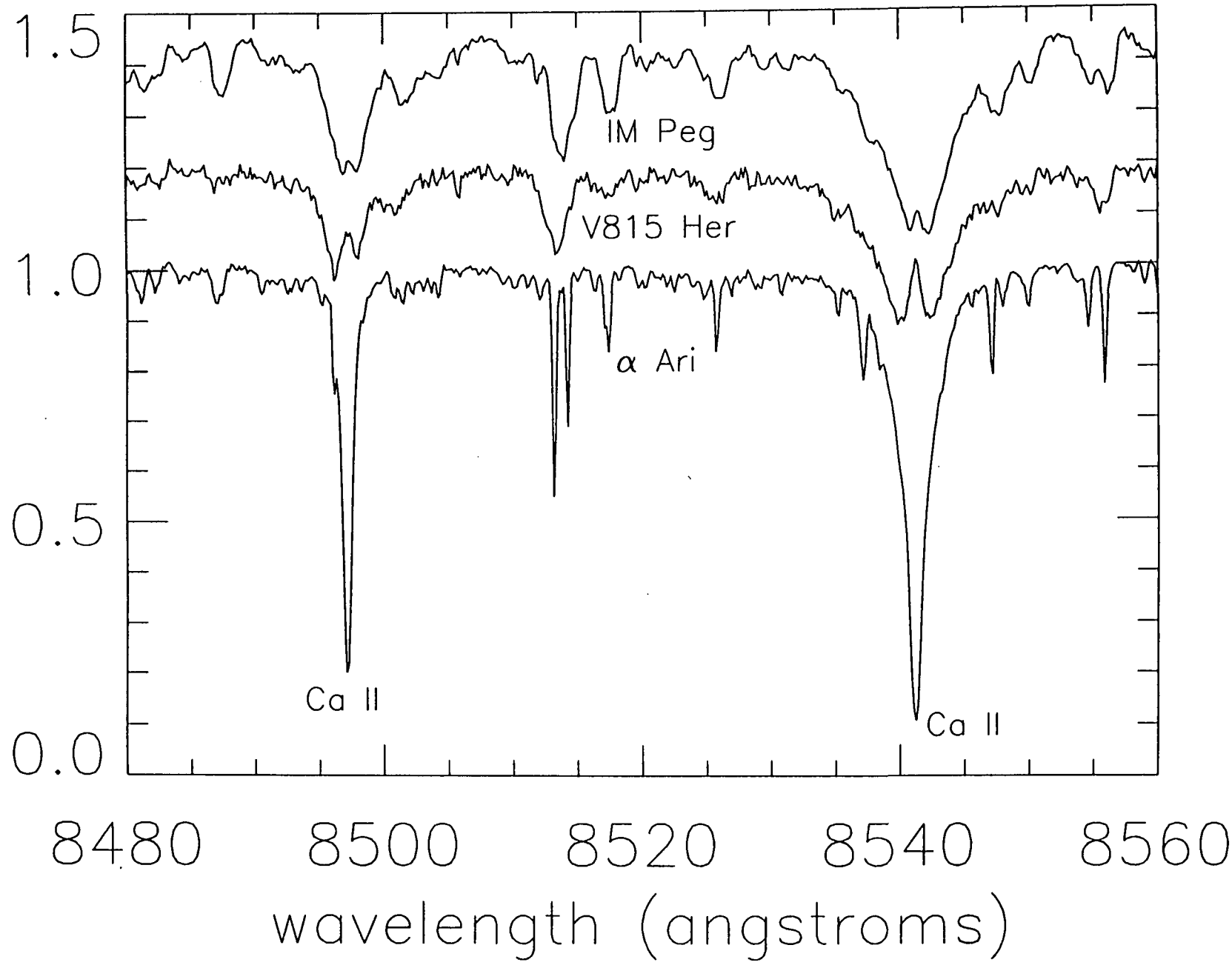
1.5
1.0
0.5
0.0
normalized intensity
IM Peg
V815 Her
α Ari
Ca II
Ca II
8480
8500
8520
8540
8560
wavelength (angstroms)

Fig. 2

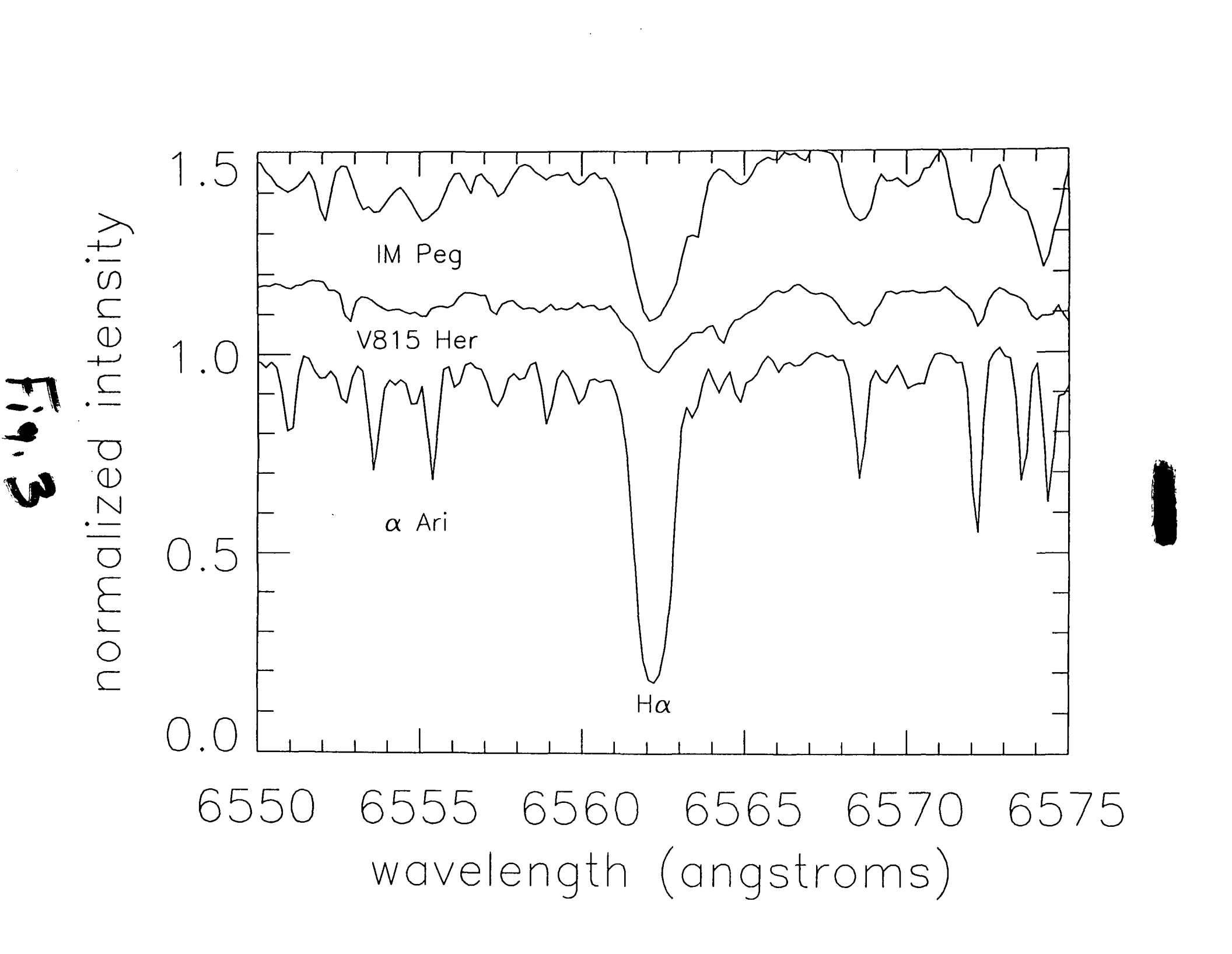
1.5
1.0
0.5
0.0
normalized intensity
IM Peg
V815 Her
α Ari
Hα
6550
6555
6560
6565
6570
6575
wavelength (angstroms)

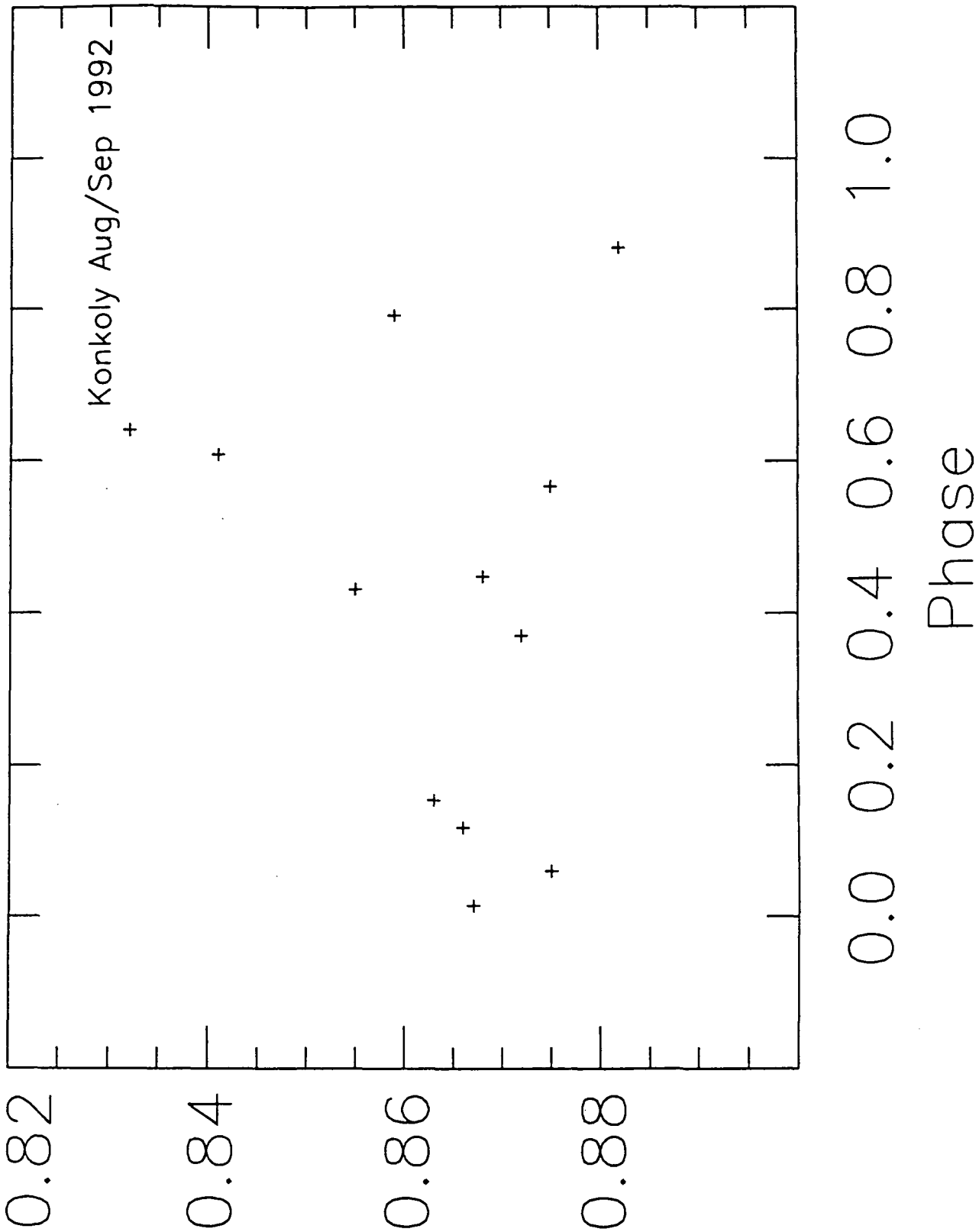
Konkoly Aug/Sep 1992
0.82
0.84
0.86
0.88
ΔV (mag)
0.0
0.2
0.4
0.6
0.8
1.0
Phase

fig. 4 Top

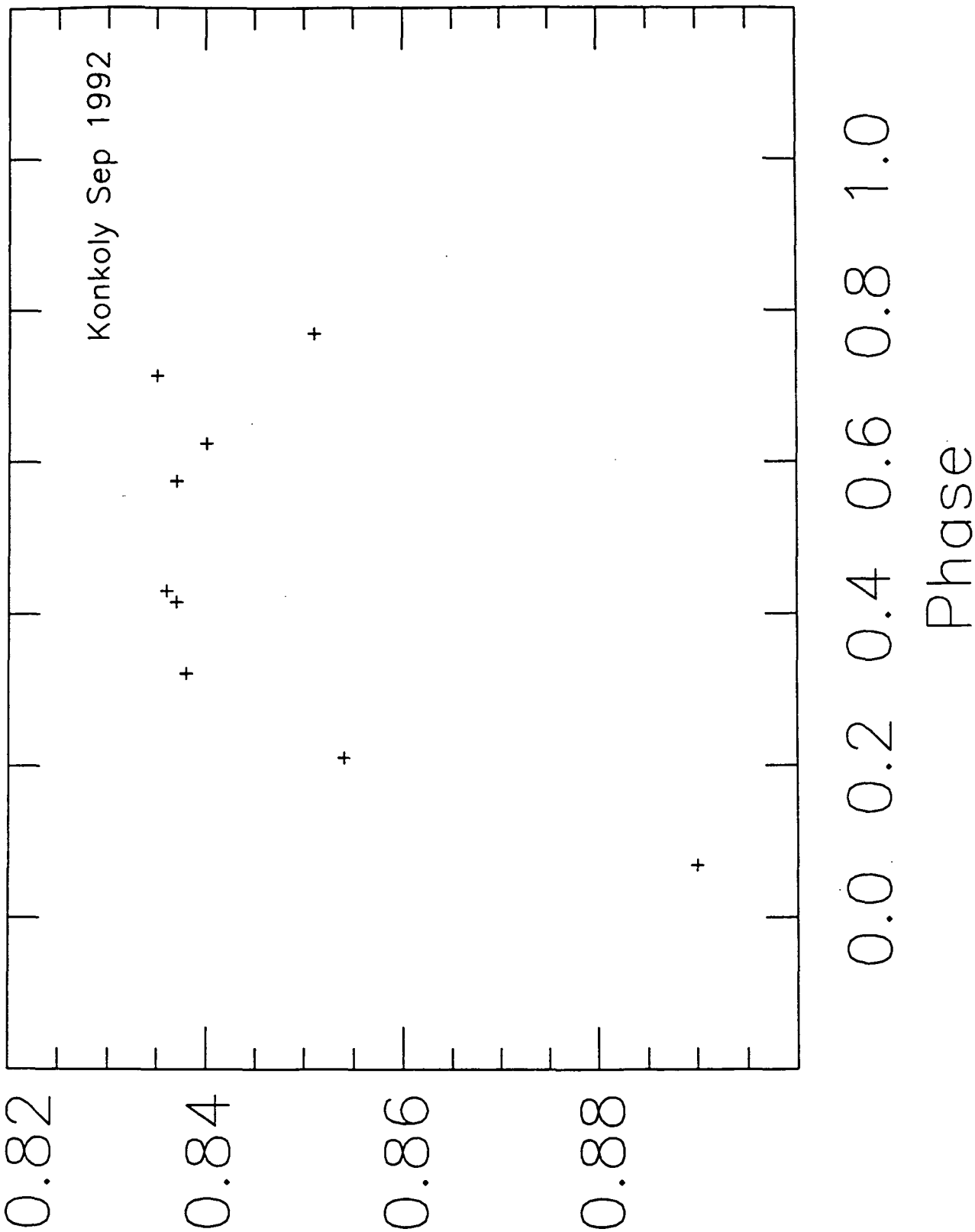

Fig. 4 Bottom

Fig. 5

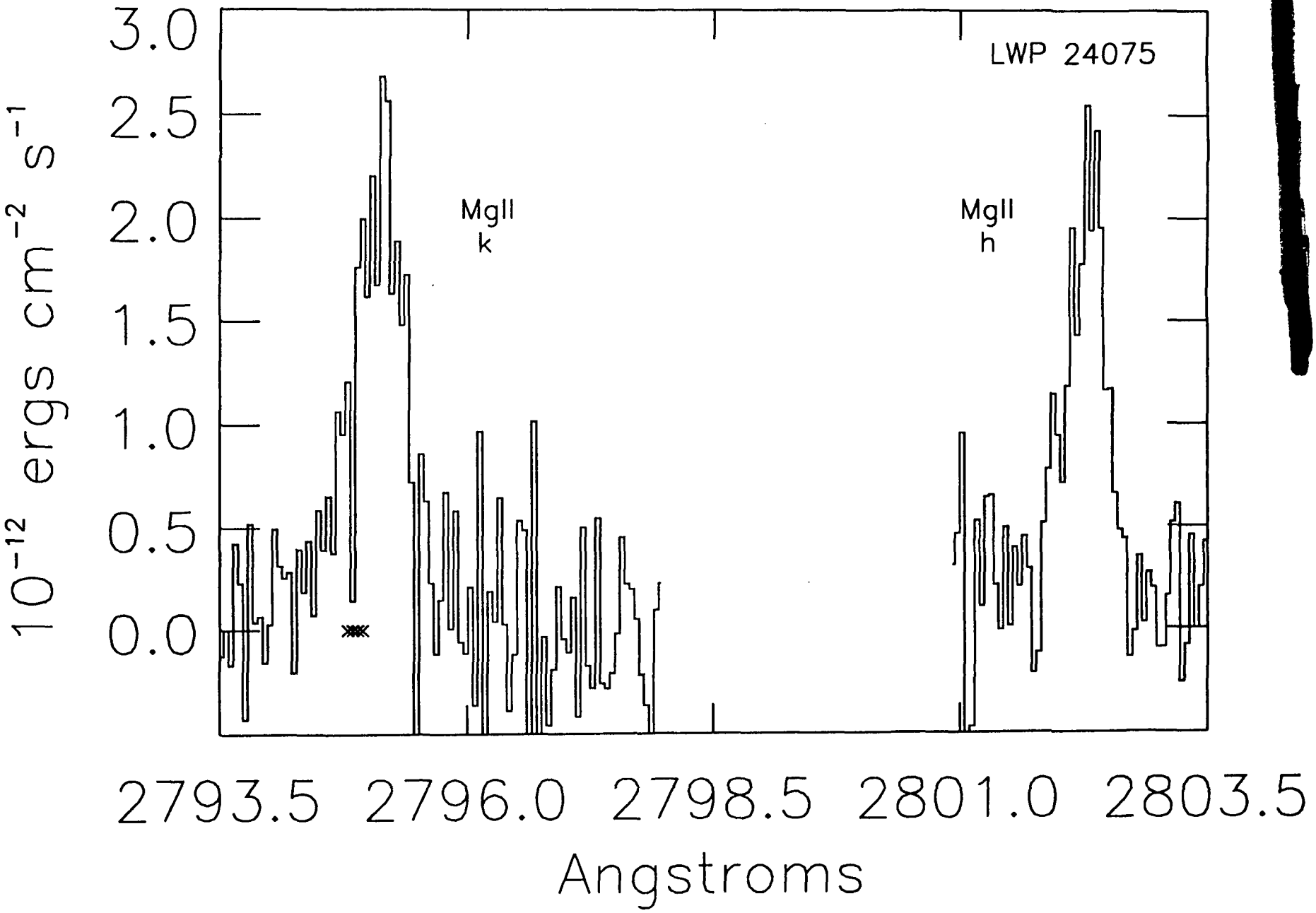
LWP 24075
MgII
k
MgII
h
3.0
2.5
2.0
1.5
1.0
0.5
0.0
10^{-12} ergs cm^{-2} s^{-1}
2793.5
2796.0
2798.5
2801.0
2803.5
Angstroms

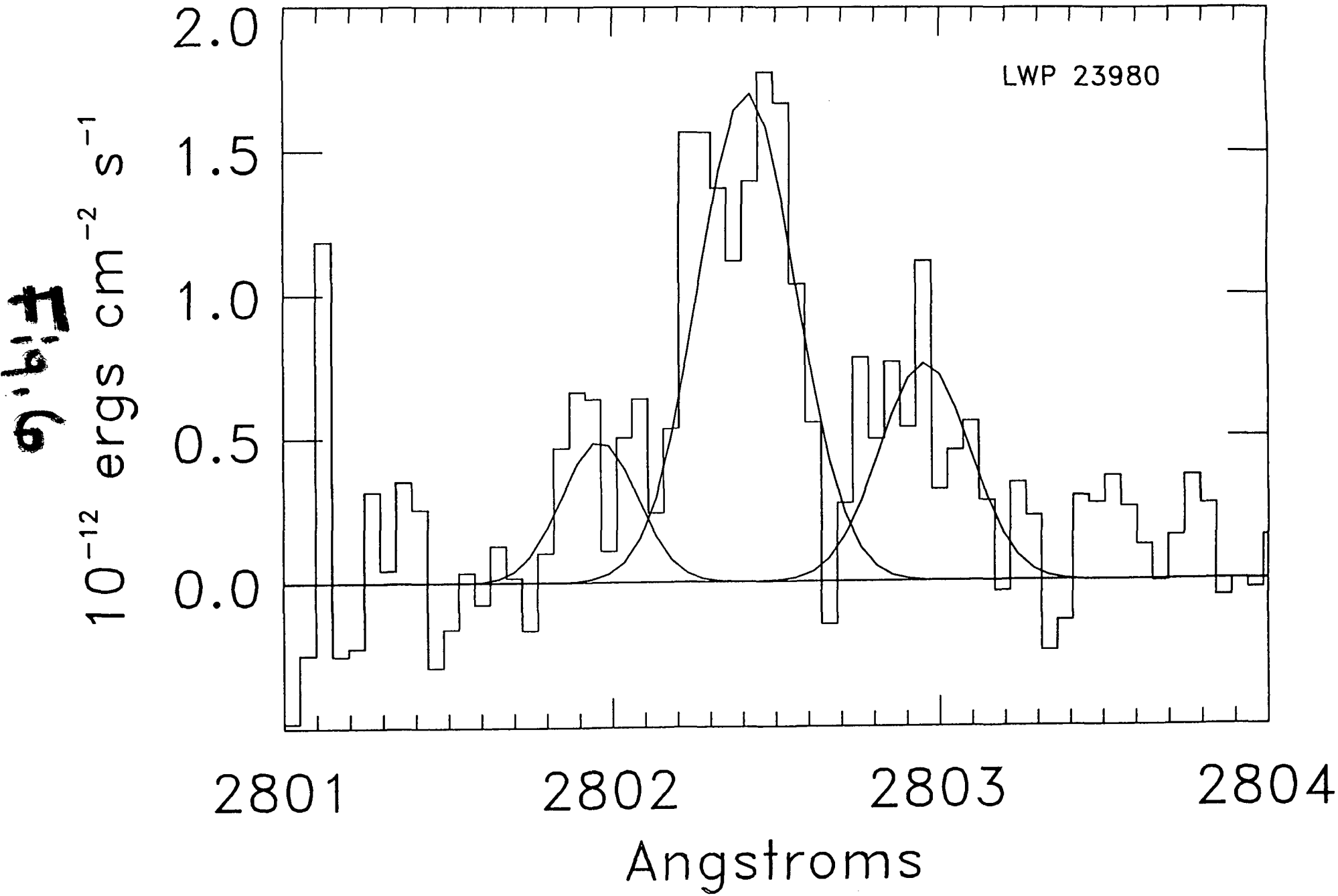
LWP 23980
2.0
1.5
1.0
0.5
0.0
10^{-12} ergs cm^{-2} s^{-1}
2801
2802
2803
2804
Angstroms

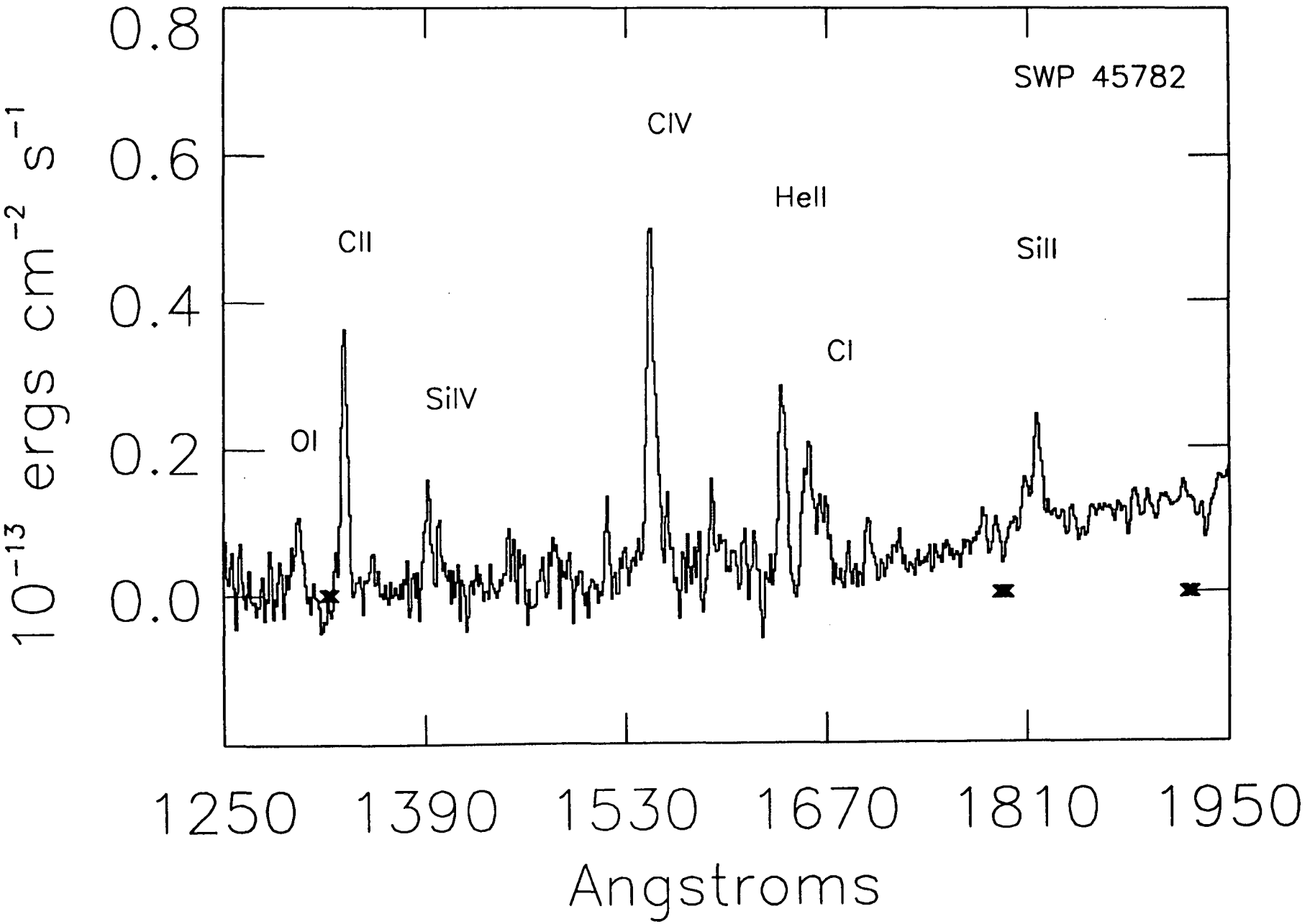
SWP 45782
CIV
HeII
CII
SiII
CI
SiIV
OI
0.8
0.6
0.4
0.2
0.0
10^{-13} ergs cm^{-2} s^{-1}
1250
1390
1530
1670
1810
1950
Angstroms

Fig. 7

HeII
CI
SiII
SiIV
CII
OI
2.5
2.0
1.5
1.0
0.5
0.0
10^{-13} ergs cm^{-2} s^{-1}
0.0
0.2
0.4
0.6
0.8
1.0
Phase

Fig. 8 Top

Fig. 8 bottom

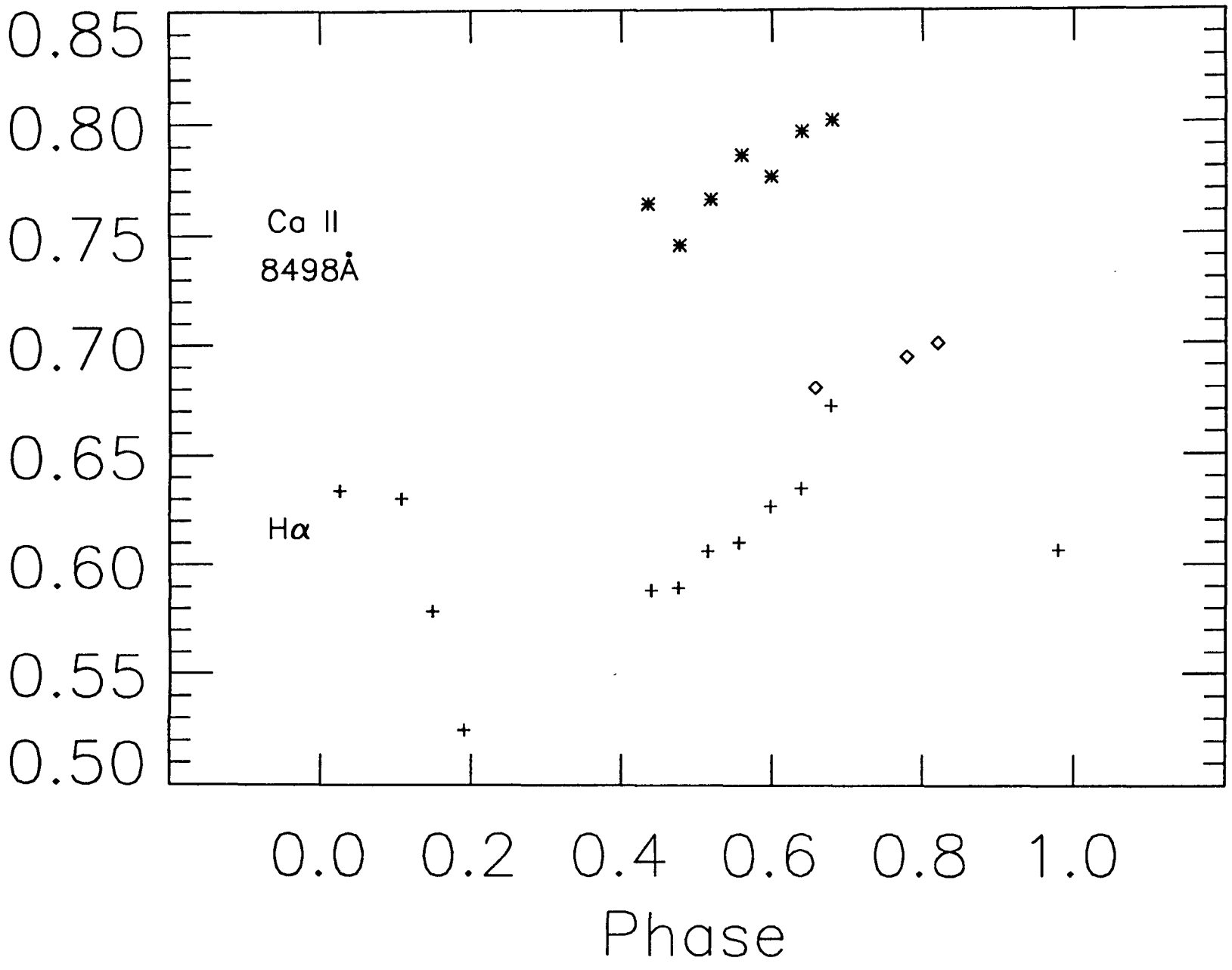
0.85
0.80
0.75
0.70
0.65
0.60
0.55
0.50
R_c
Ca II
8498Å
Hα
0.0
0.2
0.4
0.6
0.8
1.0
Phase

Fig. 9 Top

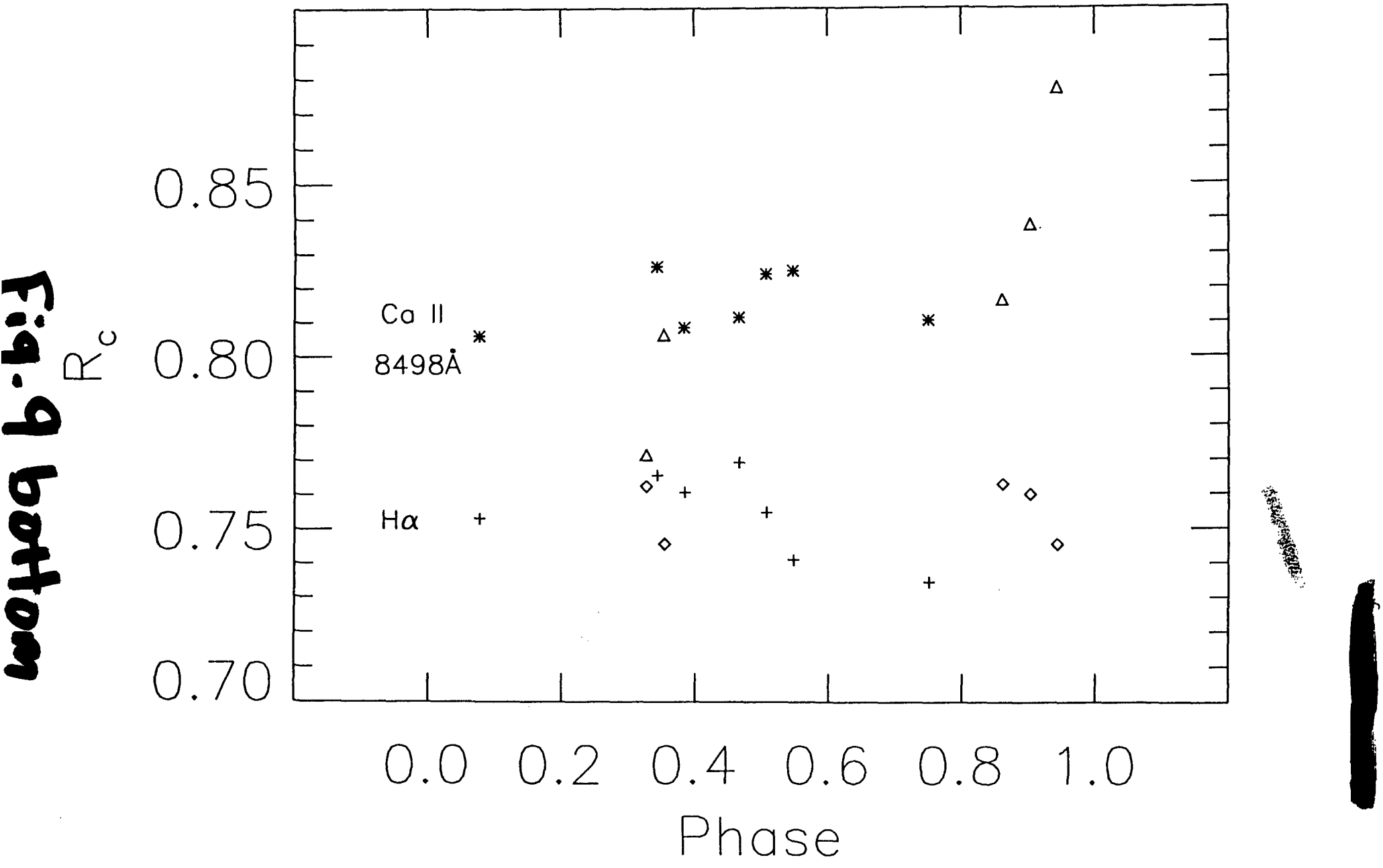

fig.9 bottom

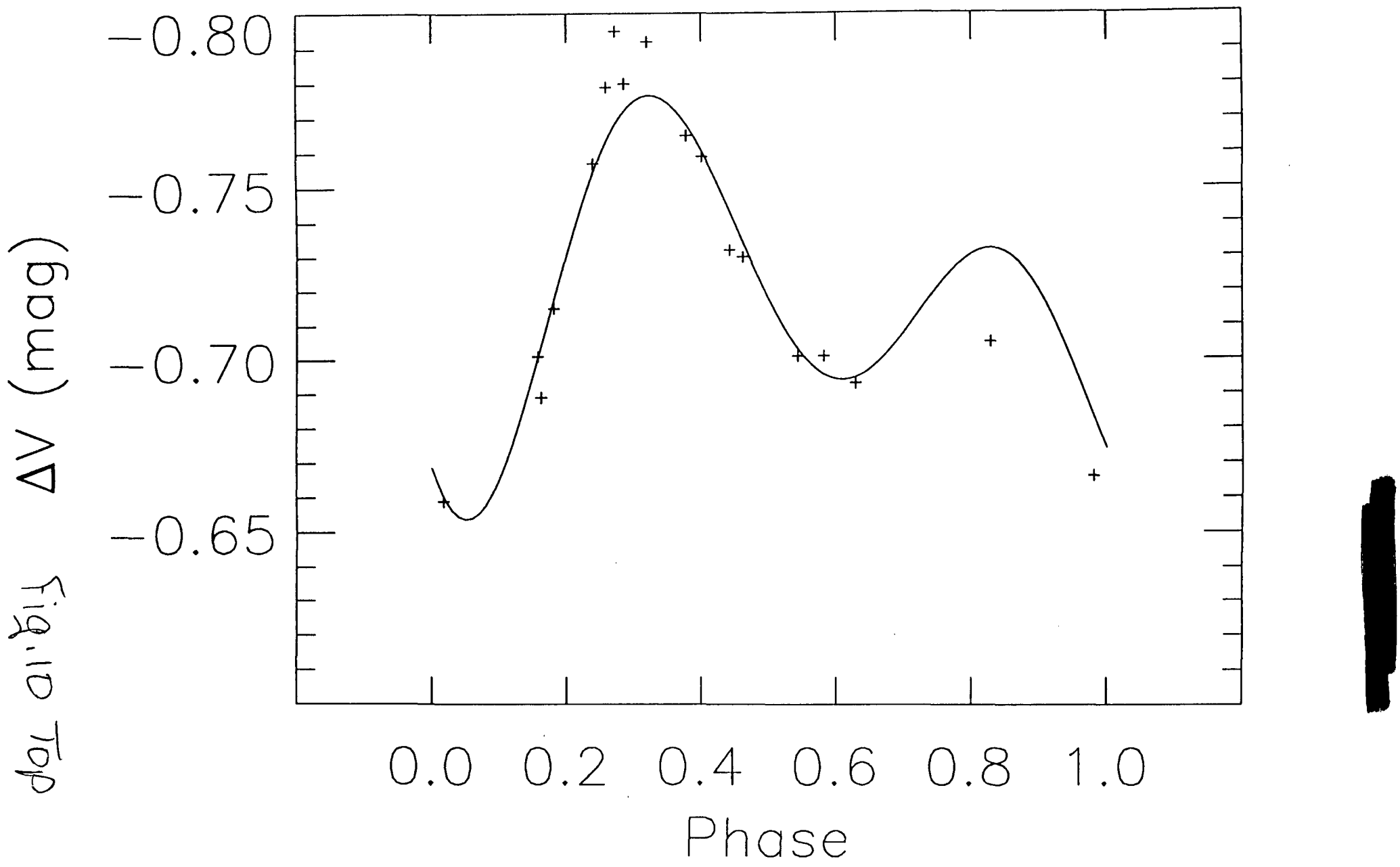

Fig. 10 top

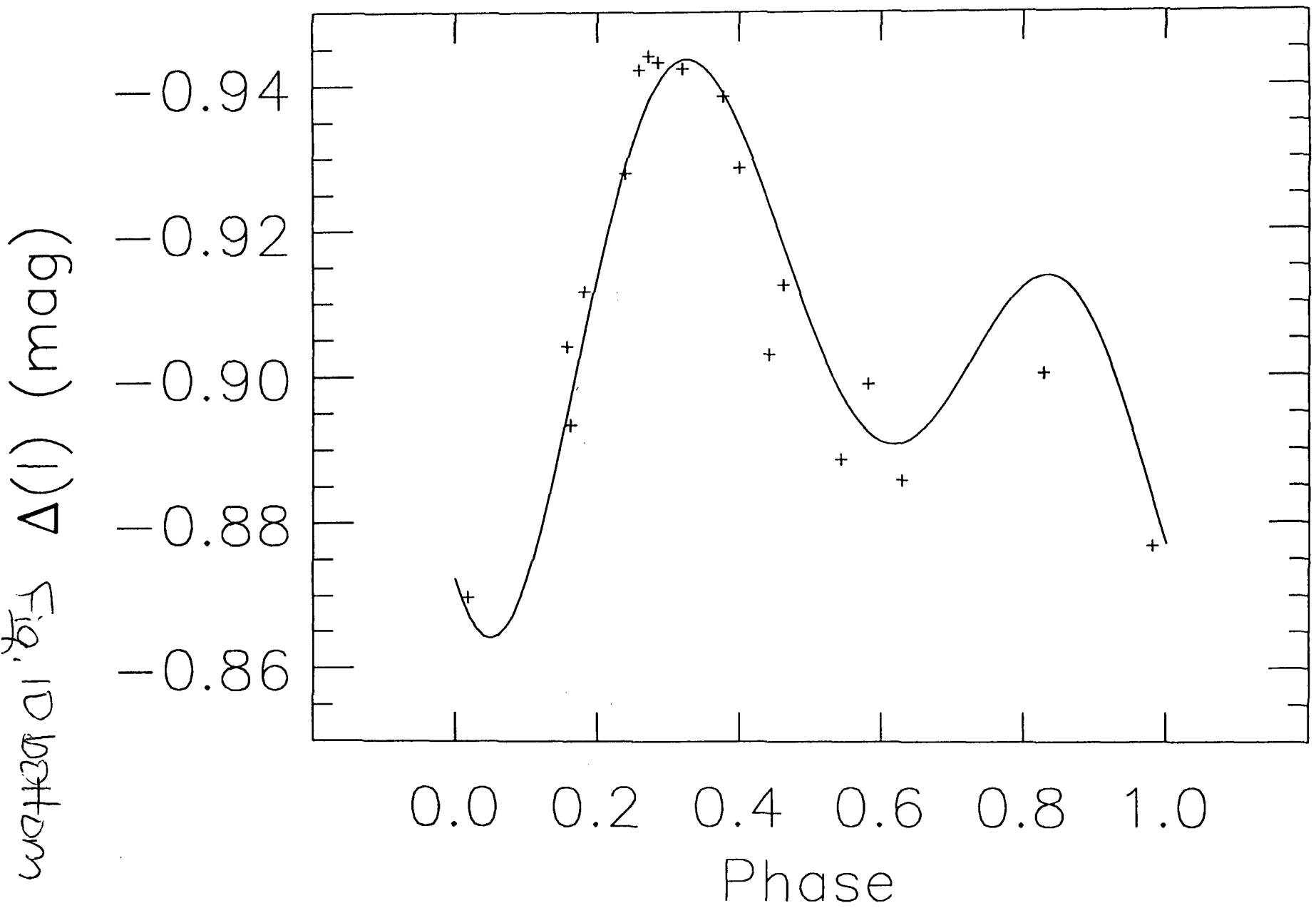
−0.94
−0.92
−0.90
−0.88
−0.86
Δ(I) (mag)
0.0
0.2
0.4
0.6
0.8
1.0
Phase

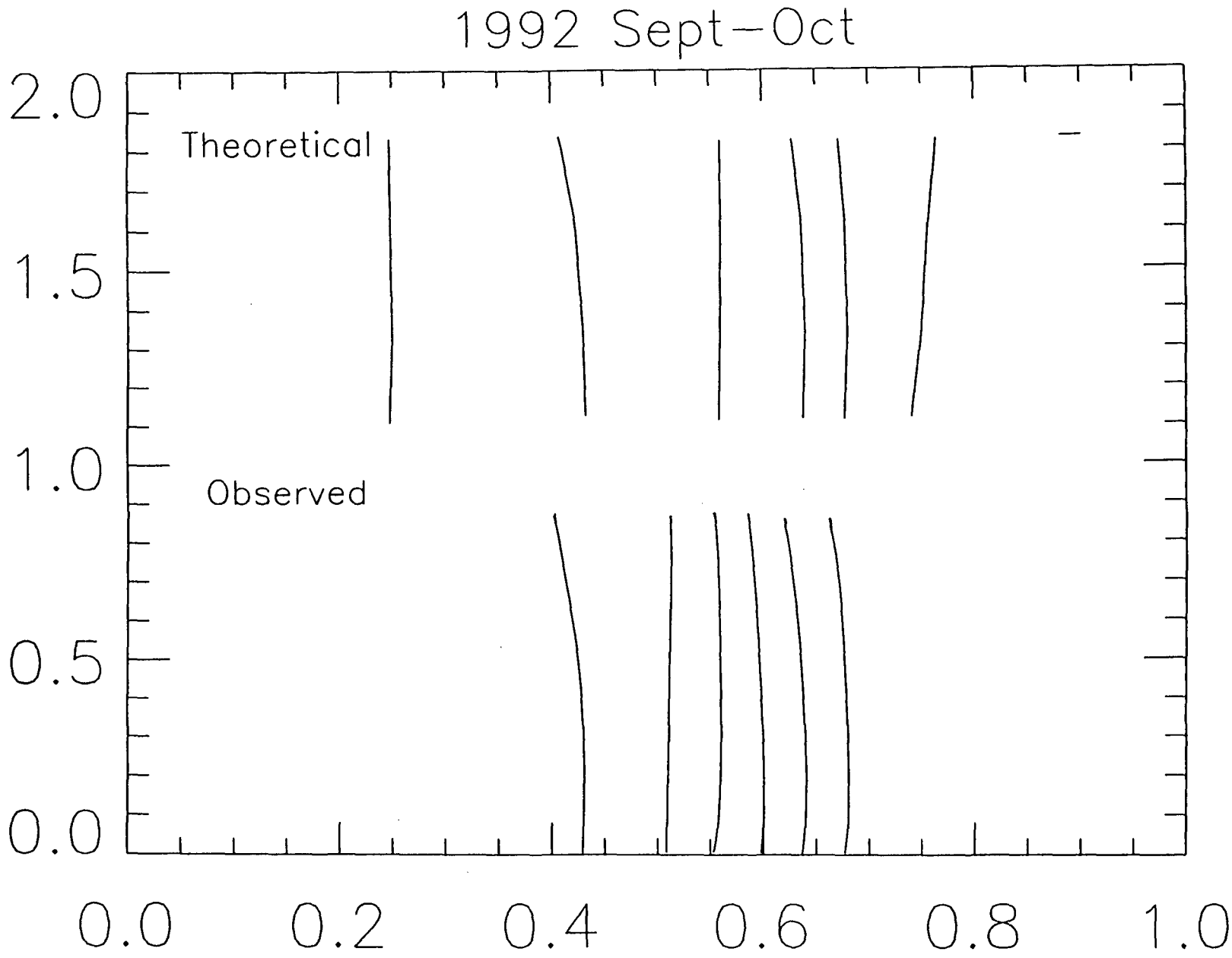
1992 Sept–Oct
Theoretical
Observed
2.0
1.5
1.0
0.5
0.0
0.0
0.2
0.4
0.6
0.8
1.0

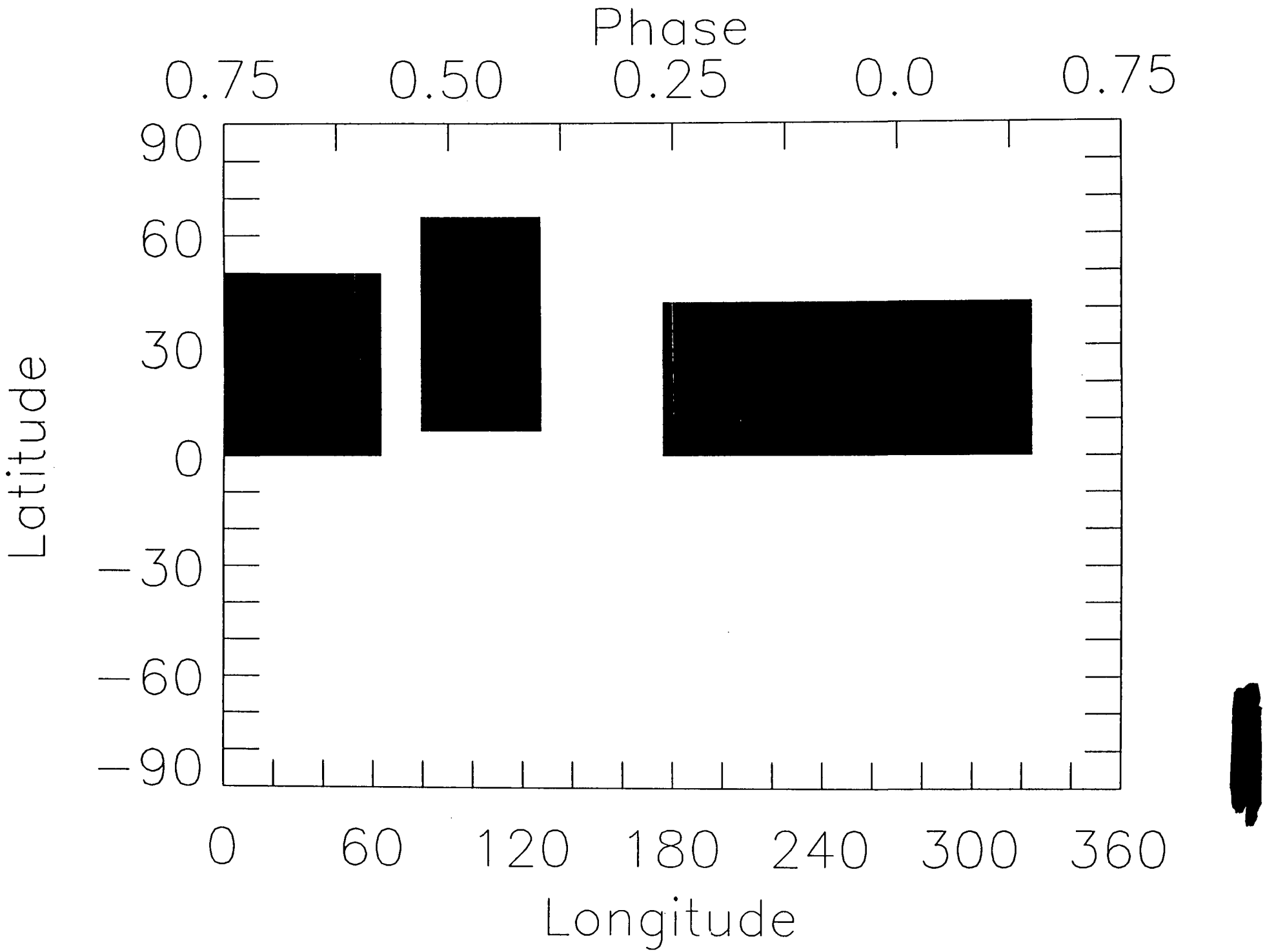
Phase
0.75
0.50
0.25
0.0
0.75
90
60
30
0
−30
−60
−90
Latitude
0
60
120
180
240
300
360
Longitude

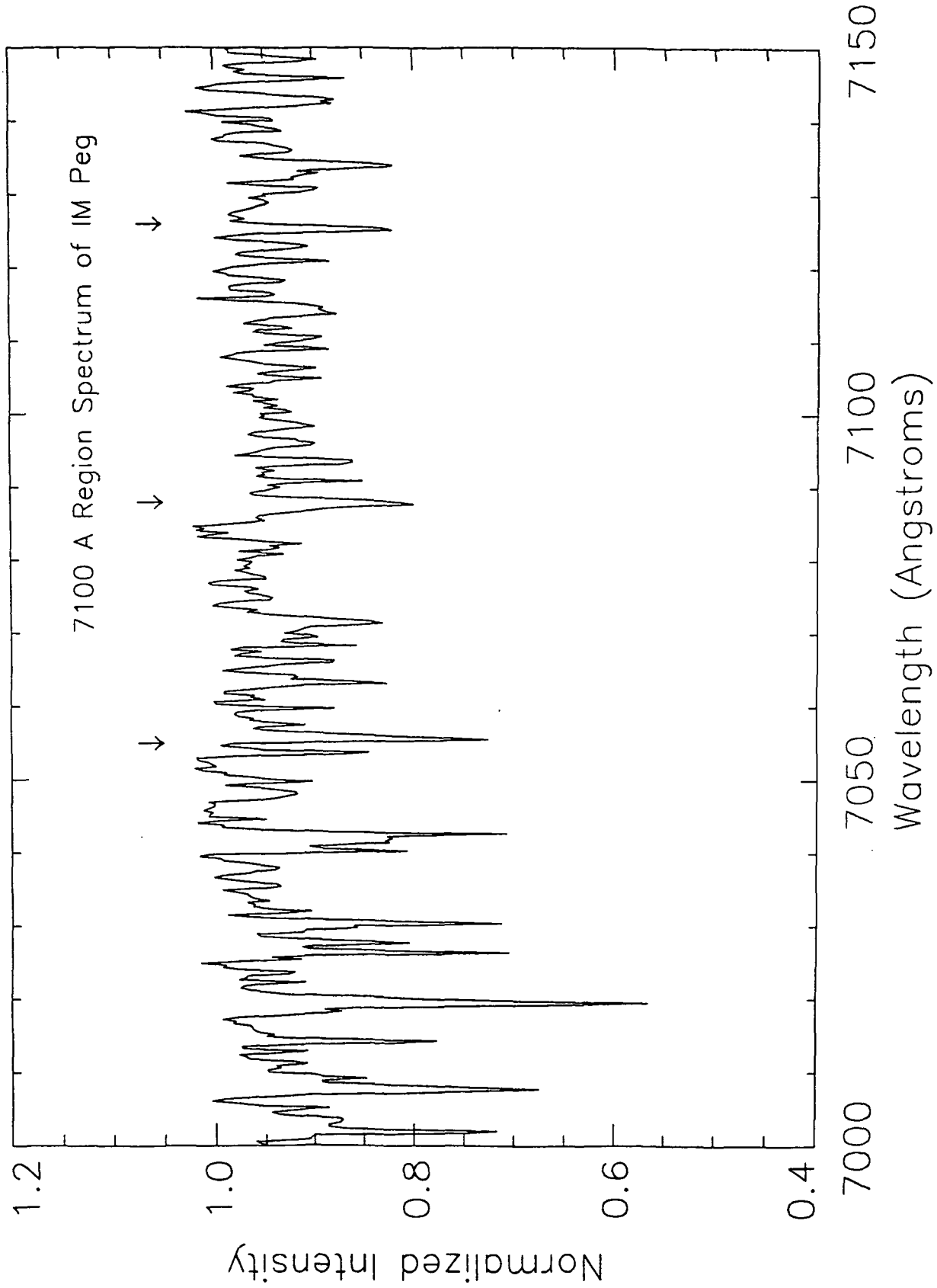
7100 A Region Spectrum of IM Peg
Normalized Intensity
1.2
1.0
0.8
0.6
0.4
7000
7050
7100
7150
Wavelength (Angstroms)

Fig. 13

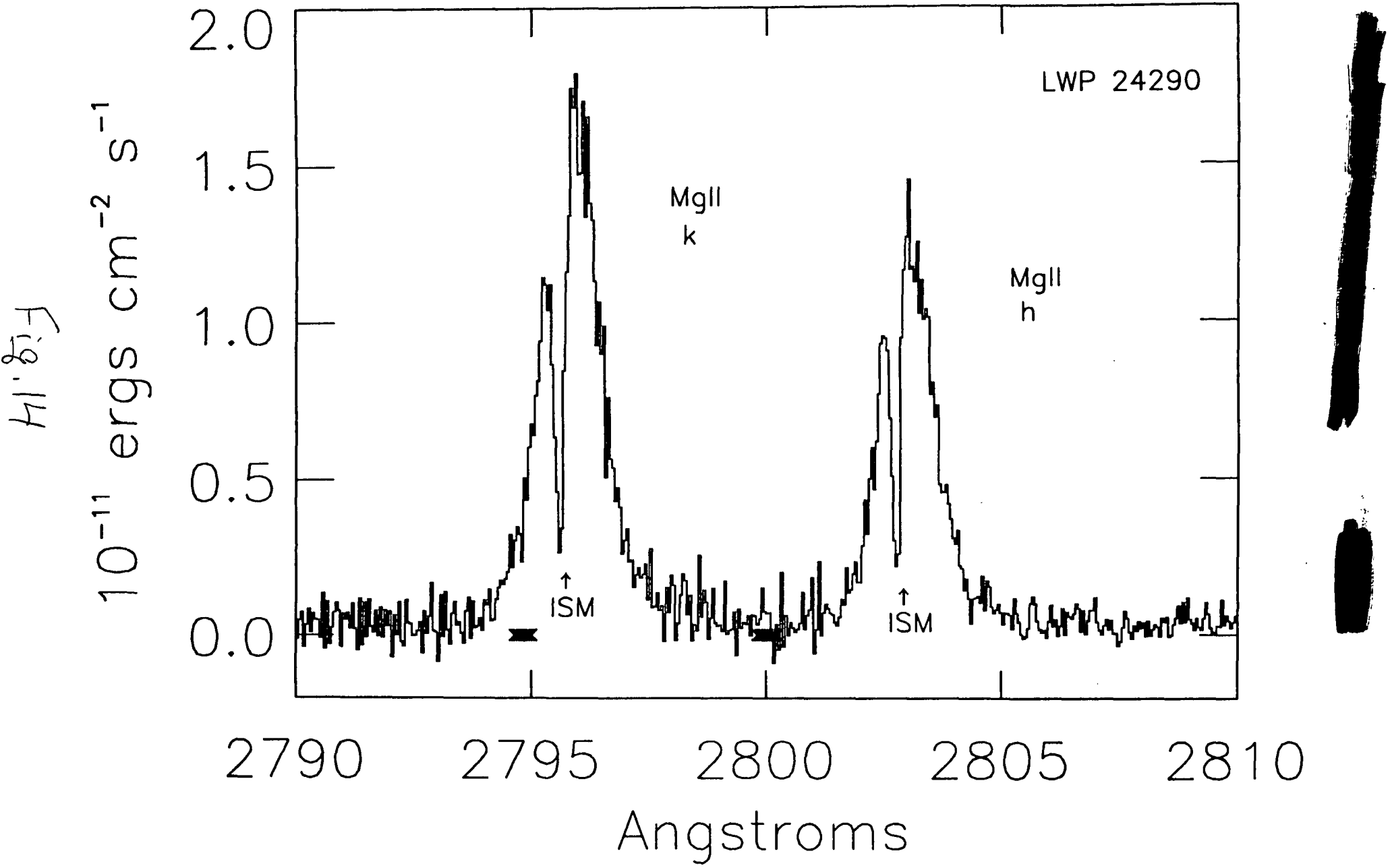
LWP 24290
MgII
k
MgII
h
ISM
ISM
2.0
1.5
1.0
0.5
0.0
10^{-11} ergs cm^{-2} s^{-1}
2790
2795
2800
2805
2810
Angstroms

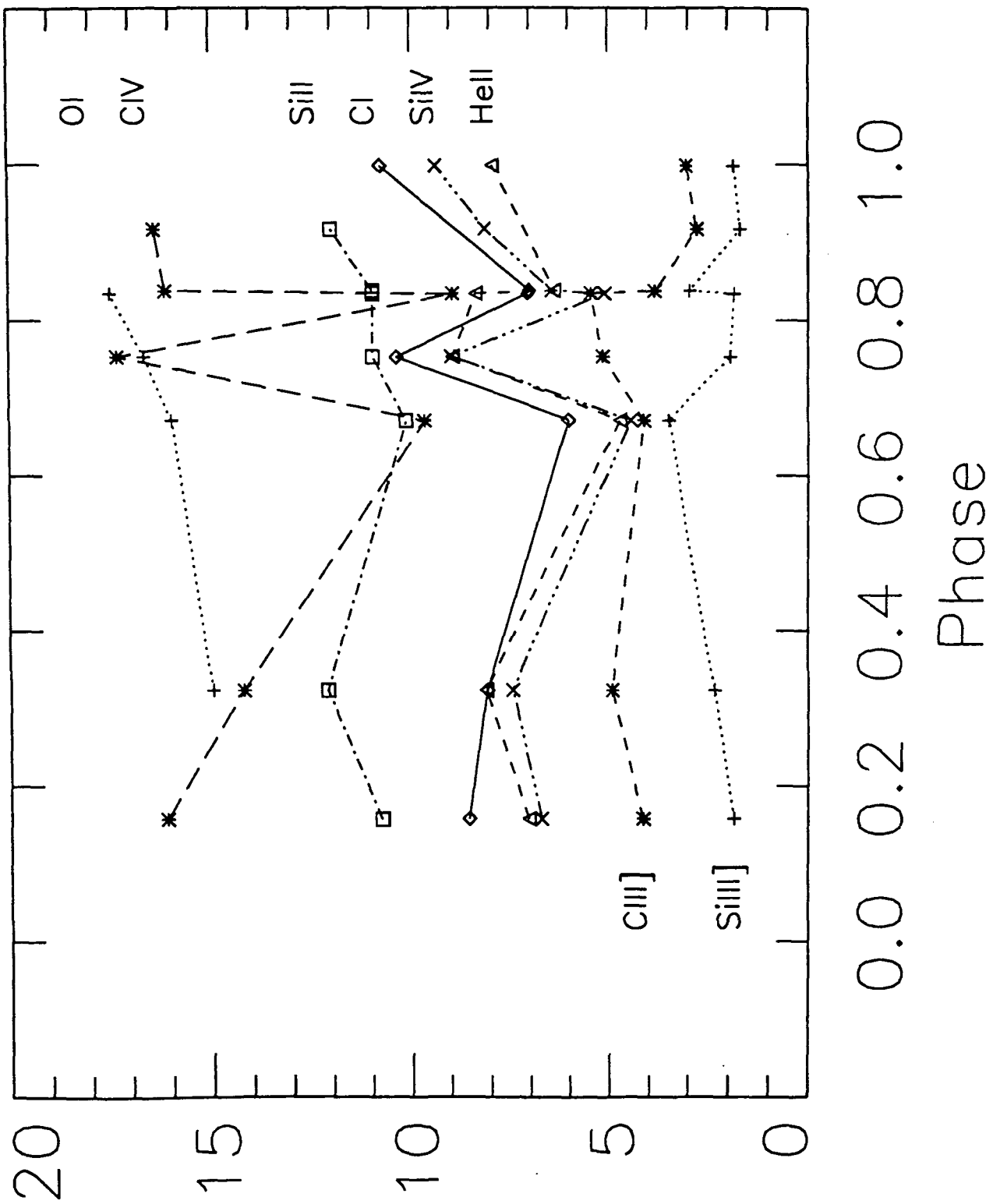

Fig. 16 Top

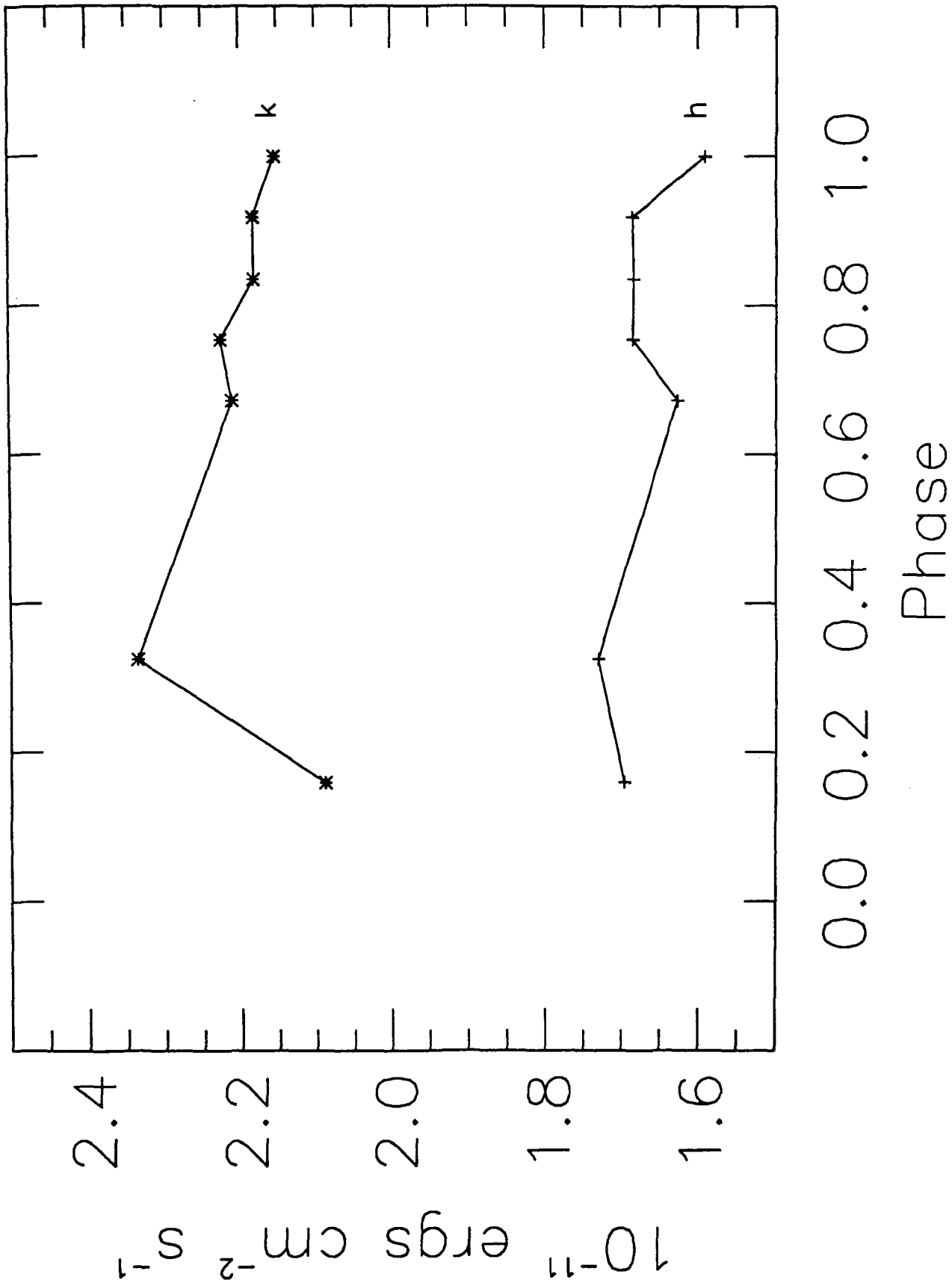

Fig. 16 bottom

REPORT DOCUMENTATION PAGE

Form Approved
OMB No. 0704-0188

1. AGENCY USE ONLY *(Leave blank)*	2. REPORT DATE	3. REPORT TYPE AND DATES COVERED
	April 1995	Contractor Report

4. TITLE AND SUBTITLE

A Multiwavelength Campaign of Active Stars with Intermediate Rotation Rates

5. FUNDING NUMBERS

8395

Code 684.1
NAS5-32487

FINAL
IN-89 p 54

6. AUTHOR(S)

Dr. Robert C. Dempsey

7. PERFORMING ORGANIZATION NAME(S) AND ADDRESS(ES)

Computer Sciences Corporation
System Science Division
4061 Powder Mill Road
Calverton, MD 20705

8. PERFORMING ORGANIZATION REPORT NUMBER

Task 4117

9. SPONSORING/MONITORING AGENCY NAME(S) AND ADDRESS(ES)

NASA Aeronautics and Space Administration
Washington, D.C. 20546-0001

10. SPONSORING/MONITORING AGENCY REPORT NUMBER

CR-199871

11. SUPPLEMENTARY NOTES

Technical Monitor: D. West, Code 684.1

12a. DISTRIBUTION/AVAILABILITY STATEMENT

Unclassified-Unlimited
Subject Category: 89
Report available from the NASA Center for AeroSpace Information,
800 Elkridge Landing Road, Linthicum Heights, MD 21090; (301) 621-0390.

12b. DISTRIBUTION CODE

13. ABSTRACT *(Maximum 200 words)*

Near-to-simultaneious ultraviolet and visual spectroscopy of two moderate $v\sin i$ RS CVn systems, V815 Herculis ($v\sin i$ = 27 km s^{-1}) and LM Pegasi ($v\sin i$ = 24 km s^{-1}), are presented along with contemporaneous $UBV\,(RI)_c$ - band photometry. These data were used to probe inhomogeneities in the chromospheres and photospheres, and the possible relationship between them. Both systems show evidence for rotationally modulated chromospheric emission, generally varying in antiphase to the photospheric brightness. A weak flare was observed at Mg II for V815 Her. In the case of IM Peg, we use photometry and spectra to estimate temperatures, sizes, and locations of photospheric spots. Further constraints on the spot temperature is provided by TiO observations. For IM Peg, the anticorrelation between chromospheric emission and brightness is discussed in the context of a possible solar-like spot cycle.

14. SUBJECT TERMS

Stars: chromospheres, binaries, late-type stars, IM Pegasi, V815 Herculis

15. NUMBER OF PAGES

53

16. PRICE CODE

17. SECURITY CLASSIFICATION OF REPORT	18. SECURITY CLASSIFICATION OF THIS PAGE	19. SECURITY CLASSIFICATION OF ABSTRACT	20. LIMITATION OF ABSTRACT
Unclassified	Unclassified	Unclassified	Unlimited

CR-199871

FINAL REPORT

"A Multiwavelength Campaign of Active Stars with Intermediate Rotation Rates"

NASA Grant NAS5-32487

Dr. Robert C. Dempsey
CSC Task 4117

This program was focused on obtaining IUE observations of chromospherically active satrs with moderate rotation rates. The IUE observations were part of larger multi-wavelength campaigns. Successful campaigns were conducted for both target stars, V815 Her and IM Peg. All the data have been obtained and analyzed for this project. The final results are presented in the attached draft manuscript, which will soon be submitted to the Astronomical Journal, after a final review is conducted by the non CSC co-authors.